Lateral frontoparietal functional connectivity based on individual sulcal morphology

Abbreviated title: Sulcal frontoparietal connectivity

Suvi Häkkinen[1,2], Willa I. Voorhies[1], Ethan H. Willbrand[1,3], Yi-Heng Tsai[1,4], Thomas Gagnant[1,5], Jewelia K. Yao[6], Kevin S. Weiner[1,2,7*], & Silvia A. Bunge[1,2*]

[1]*Department of Psychology, University of California, Berkeley, Berkeley, CA, 94720 USA*
[2]*Helen Wills Neuroscience Institute, University of California, Berkeley, Berkeley, CA, 94720 USA*
[3]*Medical Scientist Training Program, School of Medicine and Public Health, University of Wisconsin–Madison, Madison, WI, 53726 USA*
[4]*Department of Psychology and Neuroscience, University of North Carolina at Chapel Hill, Chapel Hill, NC, 27599 USA*
[5]*Medical Science Faculty, University of Bordeaux, Bordeaux, France*
[6]*Department of Psychology, Stanford University*

**shared senior authorship*

Corresponding authors: Silvia A. Bunge (sbunge@berkeley.edu) and Kevin S. Weiner (kweiner@berkeley.edu)

Keywords: neuroanatomy, sulci, neuroimaging, functional connectivity, lateral prefrontal cortex, lateral parietal cortex

Number of pages: 60
Number of figures: 4 main text (9 extended data)
Number of tables: 2 main text (2 extended data)
Number of words:
Abstract: 250
Introduction: 629
Discussion: 1475

Conflict of interest statement: The authors declare no competing financial interests.

Acknowledgments: This research was supported by NICHD R21HD100858 (Weiner, Bunge), NSF CAREER Award 2042251 (Weiner). Funding for the original data collection and curation was provided by NINDS R01 NS057156 (Bunge, Ferrer) and NSF BCS1558585 (Bunge, Wendelken). EHW was supported by the Medical Scientist Training Program Grant T32 GM140935 (Willbrand).

Abstract

A salient neuroanatomical feature of the human brain is its pronounced cortical folding, and there is mounting evidence that sulcal morphology is relevant to functional brain architecture and cognition. Recent studies have emphasized putative tertiary sulci (pTS): small, shallow, late-developing, and evolutionarily new sulci that have been posited to serve as functional landmarks in association cortices. A fruitful approach to characterizing brain architecture has been to delineate regions based on transitions in fMRI-based functional connectivity profiles; however, exact regional boundaries can change depending on the data used to generate the parcellation. As sulci are fixed neuroanatomical structures, here, we propose to anchor functional connectivity to individual-level sulcal anatomy. We characterized fine-grained patterns of functional connectivity across 42 sulci in lateral prefrontal (LPFC) and lateral parietal cortices (LPC) in a pediatric sample (N = 43; 20 female; ages 7–18). Further, we test for relationships between pTS morphology and functional network architecture, focusing on depth as a defining characteristic of these shallow sulci, and one that has been linked to variability in cognition. We find that 1) individual sulci have distinct patterns of connectivity, but nonetheless cluster together into groups with similar patterns – in some cases with distant rather than neighboring sulci, 2) there is moderate agreement in cluster assignments at the group and individual levels, underscoring the need for individual-level analyses, and 3) across individuals, greater depth was associated with higher network centrality for several pTS. These results highlight the importance of considering individual sulcal morphology for understanding functional brain organization.

Significance Statement

A salient, and functionally relevant, feature of the human brain is its pronounced cortical folding. However, the links between sulcal anatomy and brain function are still poorly understood – particularly for small, shallow, individually variable sulci in association cortices. Here, we explore functional connectivity among individually defined sulci in lateral prefrontal and parietal regions. We find that individual sulci have distinct patterns of connectivity but nonetheless cluster together into groups with similar connectivity – in some cases spanning lateral prefrontal and parietal sulci. We further show that the network centrality of specific sulci is positively associated with their depth, thereby helping to bridge the gap between individual differences in brain anatomy and functional networks leveraging the sulcal anatomy of the individual.

Introduction

Understanding the complex relationships among neuroanatomical features, functional brain network architecture, and cognition is a major goal in neuroscience. Lateral prefrontal (LPFC) and parietal (LPC) cortices are intriguing targets of exploration as they have expanded substantially across evolution and are centrally involved in high-level cognitive abilities, such as reasoning (Aichelburg et al., 2016; Krawczyk et al., 2011; Luria, 1966; Roca et al., 2010; Stuss & Knight, 2013; Woolgar et al., 2010; Vendetti & Bunge, 2014). Previous work has characterized functional connectivity between LPFC and LPC by either seeding nodes of functional networks or via data-driven parcellation of cortical areas (Yeo et al., 2011; Braga and Buckner, 2017; Dixon et al., 2018; Duncan et al., 2020; Gordon et al., 2020; Murphy et al., 2020; Gilmore et al., 2021). While these approaches have been valuable, the areal or network definitions can vary simply based on the combination of data used – with further discrepancies depending on whether analyses are conducted at the group or individual level. As such, analysis decisions (multimodal vs. unimodal, group vs. individual participant) directly influence the conclusions of these studies, resulting in disagreements regarding areal definitions in association cortices and mismatches between parcellations at the group and individual levels (Gordon et al., 2017; Seitzman et al., 2019; Gordon and Nelson, 2021; Smith et al., 2021).

On the contrary, sulci do not move and their locations have been proposed to serve as a coordinate space specific to the individual (Miller et al., 2021). Anchoring network analyses to sulci that can be identified in each individual may thus circumvent these disagreements and mismatches, providing the opportunity to glean network-level insight from individuals' local sulcal anatomy. Additionally, seeding analyses in sulci that are variable across individuals can also provide novel insights into new clusters that are cortically distant, indicating that the presence or absence of sulci is functionally meaningful at the network

level in an individual hemisphere (Lopez-Persem et al., 2019). Here, we focused on functional connectivity patterns within and between LPFC and LPC sulci during performance of a reasoning task, as recent work shows relationships between reasoning scores and morphological features of LPFC sulci, including the depths of small, shallow, and evolutionarily new sulci (termed putative tertiary sulci, or pTS, throughout the manuscript; Voorhies et al., 2021; Willbrand et al., 2023a, 2023c). We conducted four types of analyses. We report five main findings from group-level clustering analyses, with moderate agreement at the individual level. First, the three pTS in LPFC highlighted by our previous study clustered separately from other sulci. Second, some pTS in LPFC and LPC clustered together. Third, inferior portions of the intraparietal sulcus (IPS) clustered separately from more dorsal portions of the IPS, which clustered with the inferior frontal sulcus (ifs). Fourth, the superior frontal sulcus (sfs) clustered with a subset of branches of the superior temporal sulcus (sts) and pTS in inferior frontal cortex. Fifth, newly identified pTS in LPC clustered by themselves.

Additionally, we discovered a novel relationship between sulcal anatomy and functional connectivity. For all three of the LPFC pTS we tested bilaterally, the depth of the sulcus in one hemisphere was positively correlated with its network centrality, controlling for age and multiple comparisons. Exploratory analyses further revealed positive depth-centrality associations for two of three LPC pTS tested: left and right aipsJ and the recently identified right slocs-v (Willbrand et al., 2023c). These anatomically informed analyses provide insights regarding the functional brain architecture underlying reasoning that can serve as a foundation for future studies across age groups and clinical populations implementing analyses that are specific to the sulcal anatomy of the individual. These results build on the small but growing body of evidence in favor of hypothesized links between sulcal morphology and functional brain networks, which we discuss at the end of the paper.

Materials and Methods

Participants

Participants were selected from the Neurodevelopment of Reasoning Ability (NORA) dataset (Wendelken et al., 2011, 2016). Participants were all right-handed native English speakers, ranging in age from 7 to 18 (**Table 1**); for additional demographic and socioeconomic information see **Extended Data Table 1-1**. 25/43 of these participants were also included in the prior morphological study (Voorhies et al., 2021). All participants underwent preliminary screening as part of the NORA study to include only right-handed, neurotypical children and adolescents. Participants and their parents gave their informed assent and/or consent to participate in the study, which was approved by the Committee for the Protection of Human Participants at the University of California, Berkeley.

Participants were selected from the NORA study based on screening for usable T1 and fMRI data on any assessment, using MRIQC (23.1.0, Esteban et al., 2017) and manual inspection for scanner artifacts using fsleyes. For fMRI, we required three complete runs of fMRI with 165 volumes and estimated gross motion measured by mean framewise displacement < 0.5 mm (Power et al., 2014), and runs combined > 5 min worth of frames free from significant motion (framewise displacement < 0.5 mm or DVARS < 1.5). These criteria led us to retain 46% (49/107) of participants. Of the 49 participants with fMRI passing our quality criteria, two did not have LPFC labels, and four were excluded for absent sulcal components (1 rh.pimfs, 3 lh.slocs-v). Thus, 43 participants with all sulci present in both hemispheres were included in our analyses.

The age and gender distributions of these participants are reported in **Table 1**, along with their performance on a standard test of reasoning (Wechsler Intelligence Scale for Children (WISC-IV) Matrix Reasoning task; Wechsler, 1949), degree of head motion, and

amount of high-quality fMRI data used in analyses. See additional participant demographics in **Extended Table 1-1**.

Table 1. Participant characteristics (mean, range)

Age (years)	14.26 (7.12–18.86)
Gender (female/male)	20/23
Matrix reasoning (t-score)*	58.43 (43.00 - 81.00)
Head motion (mean framewise displacement in mm)	0.22 (0.08–0.43)
fMRI data after censoring (min)	12.67 (5.47–16.20)

*Score not available for one participant.

fMRI task

Functional connectivity was measured based on fMRI data collected during performance of a relational reasoning task (described in Wendelken et al., 2011). In short, participants viewed arrays of four visual stimuli on each trial. In first-order reasoning blocks, they judged whether the pair of stimuli in each row shared a particular feature: shape or fill pattern (e.g., on a shape trial, judging that an orange triangle and a yellow triangle match on shape). In second-order reasoning blocks, they judged whether two pairs of stimuli matched according to the same feature - that is, the shape or fill pattern (e.g., judging that two circles and two squares both match according to shape).

MRI acquisition

Brain imaging data were originally collected on a Siemens 3T Trio system at the University of California Berkeley Brain Imaging Center. T1-weighted MPRAGE anatomical scans (TR = 2300 ms, TE = 2.98 ms, 1 × 1 × 1 mm voxels) were acquired for cortical morphometric

analyses. fMRI data were acquired using gradient-echo EPI sequence, TR = 2000 ms, TE = 25 ms, 33 axial slices, 2.0 × 1.8 × 3.0 mm voxels, no interslice gap, flip angle = 90°, field of view = 230 mm, 120 volumes per run). The fMRI experiment consisted of three runs of 5 min 25 s each of the relational matching task described above, with 90-s blocks consisting of 6-s trials, separated by 20-s rest blocks. The current analyses focus on functional connectivity across both types of task blocks, as well as rest blocks; thus, we measured overall connectivity in the context of a reasoning task.

Cortical surface reconstruction

FreeSurfer's automated segmentation tools (Dale et al., 1999; Fischl and Dale, 2000) (FreeSurfer 7.1.0) were used to generate cortical surface reconstructions. Each anatomical T1-weighted image was segmented to separate gray from white matter, and the resulting boundary was used to reconstruct the cortical surface for each participant (Dale et al., 1999; Wandell et al., 2000). Each reconstruction was visually inspected for segmentation errors, and these were manually corrected when necessary.

Manual labeling of LPFC and LPC sulci

To investigate the network defined by the LPFC–LPC sulcal features, 42 sulci (10 LPFC and 11 LPC in each hemisphere; **Table 2**) were manually defined for each participant and hemisphere. These anatomical features were defined according to the most recent atlas by Petrides (Petrides, 2019) and our recent findings (Willbrand et al., 2023c). The anatomical locations are illustrated in **Figure 1**, and all 1806 sulcal definitions in all participants can be found in **Extended Data Figure 1-1**. The location of each sulcus was confirmed by trained independent raters (W.I.V., E.H.W., J.Y., T.G., Y.T.) and finalized by a neuroanatomist (K.S.W.). Surface vertices for each sulcus were selected using tools in FreeSurfer, guided by

the pial and smoothwm surfaces (Weiner et al., 2018; Miller et al., 2021), and saved as surface labels for vertex-level analysis.

Table 2. Sulcal definitions in LPFC and LPC

Lobe	Name	Abbreviation
LPFC	inferior frontal sulcus	*ifs*
LPFC	superior frontal sulcus – posterior	*sfs-p*
LPFC	superior frontal sulcus – anterior	*sfs-a*
LPFC	posterior middle frontal sulcus – posterior	*pmfs-p*
LPFC	posterior middle frontal sulcus – intermediate	*pmfs-i*
LPFC	posterior middle frontal sulcus – anterior	*pmfs-a*
LPFC	para-intermediate frontal sulcus	*pimfs**
LPFC	ascending ramus of the lateral fissure	*aalf*
LPFC	pretriangular sulcus	*prts*
LPFC	lateral frontomarginal sulcus	*lfms*
LPC	sulcus of Brissaud	*sB*
LPC	intermediate parietal sulcus – posterior	*pips*
LPC	transverse occipital sulci – medial	*mTOS*
LPC	transverse occipital sulcus – lateral	*lTOS*
LPC	paroccipital intraparietal sulcus	*IPS-PO*
LPC	intraparietal sulcus	*IPS*
LPC	three different branches of the caudal superior temporal sulcus (anterior to posterior)	*cSTS1,2,3*
LPC	intermediate parietal sulcus of Jensen – anterior	*aipsJ*
LPC	supralateral occipital sulcus – ventral	*slocs-v*

*The pimfs can have 0, 1, or 2 components; dorsal and ventral components have been combined into one label for the present study, as in Voorhies et al. (2021) and Yao et al. (2023).

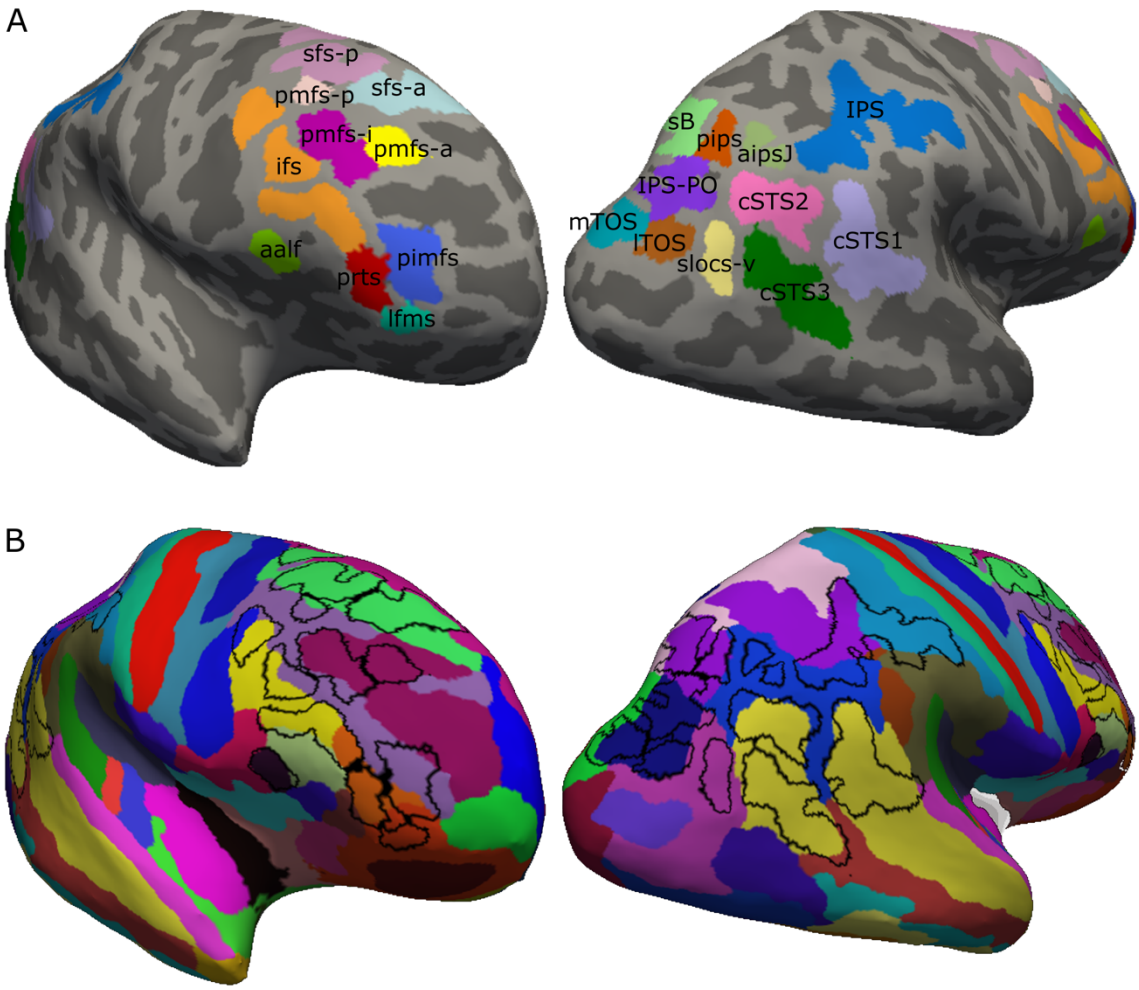

Figure 1. Lateral prefrontal (LPFC) and lateral parietal (LPC) sulcal definitions. (A) Manual sulcal definitions on an example cortical surface reconstruction of a right hemisphere. Definitions of all participants are shown in **Extended Data Figure 1-1**. (B) Manual definitions (black outlines) overlaid on the Destrieux atlas generated using automated methods (Fischl, 2004; Destrieux et al., 2010). Note that many of the LPFC and LPC sulci (black outlines) do not align with the automatic definition of these structures,

indicating that manually defined sulci are necessary to explore the functional connectivity of LPFC and LPC sulci in individual participants.

Morphological features

Sulcal depth was defined by maximum 'sulc' value estimated by FreeSurfer for each sulcal label. Sulcal area was defined by total surface area (mris_anatomical_stats).

fMRI data preprocessing

We drew the raw fMRI data for included participants from the previous dataset, and preprocessed them de novo. Here, we used fMRIprep version 21.0.1 (Esteban et al., 2019)[RRID:SCR_016216], which is based on Nipype 1.6.1 (Gorgolewski et al., 2011)[RRID:SCR_002502]. Each T1w (T1-weighted) volume was corrected for intensity non-uniformity using N4BiasFieldCorrection v2.3.3 (Tustison et al., 2010) and skull-stripped using antsBrainExtraction.sh v2.1.0 (using the OASIS template). Brain surfaces were reconstructed using recon-all from FreeSurfer v7.1.0 (Dale et al., 1999)[RRID:SCR_001847], and the brain mask estimated previously was refined with a custom variation of the method to reconcile ANTs-derived and FreeSurfer-derived segmentations of the cortical gray-matter of Mindboggle (Klein et al., 2017)[RRID:SCR_002438]. Brain tissue segmentation of cerebrospinal fluid (CSF), white matter (WM) and gray matter (GM) was performed on the brain-extracted T1w using fast ((Zhang et al., 2001), FSL v6.0.5, RRID:SCR_002823).

For each of the three runs, the initial three volumes were excluded, functional data was slice time corrected using 3dTshift from AFNI v16.2.07 (Cox, 1996)[RRID:SCR_005927] and motion corrected using mcflirt (Jenkinson et al., 2002)(FSL v6.0.5). This was followed by co-registration to the corresponding T1w using boundary-based registration (Greve and Fischl, 2009) with six degrees of freedom, using bbregister (FreeSurfer v7.1.0). Motion correcting transformations, BOLD-to-T1w transformation and

T1w-to-template (MNI) warp were concatenated and applied in a single step using antsApplyTransforms (ANTs v2.1.0) using Lanczos interpolation. The functional series were then sampled to native mid-grey matter surface by averaging across the cortical ribbon. Physiological noise regressors were extracted applying CompCor (Behzadi et al., 2007). For aCompCor, six principal components were calculated within the intersection of the subcortical mask and the union of CSF and WM masks calculated in T1w space, after their projection to the native space of each functional run. Framewise displacement (Power et al., 2014) was calculated for each functional run using the implementation of Nipype.

Following preprocessing via fMRIPrep, fMRI data were despiked (AFNI 3Ddespike, default c1 = 2.5, c2 = 4.0) and bandpass filtered (AFNI 3DBandpass, 0.008–0.1 Hz). Nuisance regressors were filtered and regressed from the timeseries (Nilearn image.clean_img). The confounds included linear trends, the first 5 aCompCor components, and 24 motion parameters (Friston et al., 1996).

Measurement of sulcal functional connectivity and correction for spatial autocorrelations

We computed functional connectivity between all 42 sulcal labels for each participant. To this end, the mean timeseries of all vertices in each sulcal label were averaged using custom code (libraries NiBabel, NumPy). Functional connectivity was measured by pairwise Pearson correlations between the timeseries for each sulcal label across all three runs, excluding frames associated with large motion spikes (framewise displacement < 0.5 or DVARS < 1.5). The correlation values were subsequently normalized to z-scores via a Fisher transformation, and then combined into a 42 × 42 inter-regional correlation matrix for each participant. The analyses were based on the full acquisition with task and rest blocks concatenated. To mitigate effects of in-scanner head motion, mean framewise displacement was residualized

from the data prior to analyses of network organization and included as a covariate in analyses on associations with age and reasoning performance.

The results featured here control for spatial autocorrelation, which may artificially inflate functional connectivity between adjacent sulcal components. Spatial autocorrelation was estimated and controlled for per participant and hemisphere as follows: 1) Functional connectivity and corresponding geodesic distances were calculated for nodes in 32k meshes (Connectome Workbench) of cortical mid-grey matter, excluding the medial wall (Python library gdist 1.0.3). 2) Spatial autocorrelation was modeled as a function defined by a rate of exponential distance-dependent decrease and the constant baseline level to which it decays, and fitted to the data divided into 1 mm bins using gradient descent, similar to Shinn et al. (2023). For all participants and hemispheres, the positive bias of adjacent connections was found to taper off at < 1 cm. To define a regressor that describes the short-distance positive bias and does not change the connectivity values of sulcal pairs at longer distances than the subject's estimated range of spatial autocorrelations, the constant baseline level was subtracted from the fitted function. 3) Minimum geodesic distance was extracted for the vertices of each sulcal label pair of the participant. 4) Based on the autocorrelation function and calculated minimum distance, each sulcal label pair was matched with the expected positive bias. 5) Association between the bias regressor and connectivity of the sulcal network was estimated for each hemisphere and participant using least squares regression. Connectivity values were then residualized for the estimated regression with the bias variable. 6) The corrected within-hemisphere connections were combined with between-hemisphere connections for further analysis.

While spatial autocorrelations are an important potential confound, correcting for them may diminish true short-distance connectivity and confound network topological

measures (Shinn et al., 2023). Thus, we also ran supplementary analyses in which we did not correct for them.

Discriminability of sulcal connectivity patterns

We performed classification analysis testing the discriminability of the sulci from one another based on their connectivity patterns. The multiclass classification problem was split into 861 binary classification problems (one-vs-one approach) (Galar et al., 2011). We chose a support vector machine (SVM) as a classifier, given the small, high-dimensional sample, and employed a linear kernel to avoid overfitting. SVMs (sklearn implementation based on LIBSVM; default regularization C = 1) were trained to discriminate each pair of sulci based on their functional connectivity fingerprint. To avoid having the classifications be driven by strong autocorrelations, the connectivity between the two sulci being tested was excluded from each binary classification, such that the classification was based on the connectivity strength between each of these two sulci and the 40 remaining sulci. Connectivity weights of each participant were normalized to [0,1], and each feature to [0,1] during cross-validation. Classification performance was assessed using leave 3 subjects out cross-validation repeated 10 times, and accuracy (the percentage of samples predicted correctly) was measured as the mean value across folds. Empirical p-values were generated against the null hypothesis that connectivity fingerprints and sulcal labels are independent, using permutation testing (100 permutations of each fold) and correcting for multiple comparisons using the Benjamini-Hochberg false discovery rate (FDR) (Benjamini and Hochberg, 1995).

Connectivity-based clustering

To detect groups of sulci with similar sulcal connectivity profiles, connectivity matrices were averaged into a mean connectivity matrix, and the mean matrix was clustered using an unsupervised community detection algorithm (Infomap) (Rosvall and Bergstrom, 2008).

Clusters were investigated at density thresholds 0.01–0.5 in steps of 0.01, preserving the indicated proportion of the strongest weights at each iteration. The representativeness of the group-level clustering at the individual subject level was assessed as follows: First, clustering was applied to individual-level networks. For each label pair, co-clustering was defined as the number of times each pair of labels was found in the same cluster, at thresholds ranging from the lowest threshold at which the sulcus was clustered with at least one other sulcus to the threshold at which all sulci were clustered into one. Co-clustering counts were collapsed into a binary estimate indicating whether the pair clustered together for at least three of the investigated thresholds. Finally, an agreement matrix described the frequency of co-clustering per sulcal pair, presented as a proportion of participants.

Sulcal associations with canonical large-scale resting-state fMRI networks

To determine how individual sulci associate with previously characterized large-scale functional networks, we assessed the similarity of each sulcus and 14 networks in the MIDB Precision Brain Atlas (Hermosillo et al., 2024), derived from probabilistic network maps from resting-state fMRI data, that were largely invariant in network topography across roughly 6000 9–10 year-olds. Network seed masks were defined at 61% probability in the atlas, producing reasonably sized seeds for connectivity analysis. The atlas labels were projected from standard space (fs_LR_32) to the native surfaces of each subject using Connectome Workbench tools and custom scripts. The mean timeseries of each network label and sulcus (same hemisphere) were then correlated as above.

Graph network metrics

Based on the 42 × 42 matrices of sulcal connectivity, we derived graph metrics for each node (sulcus) in each participant. Individual nodes were characterized using three topological measures describing their level of centrality in the LPFC-LPC sulcal network: 1) degree, or

the number of links connected to the node; 2) betweenness, or the frequency that a node is on the shortest path connecting other nodes; and 3) participation coefficient, a measure of how evenly distributed a node's connections are across clusters (Rubinov and Sporns, 2010). To account for differences in overall connectivity strength across participants, the graph analyses used binarized networks and area under curve (AUC) estimates, integrating values across 0.01–0.2 density. Participation coefficient was calculated using the group-level clusters shown in **Figure 2B**.

For each graph metric, the sulcal components scoring consistently high across subjects were defined by comparison to the mean of all values for a given participant using two-tailed paired t-tests, and FDR-corrected for multiple comparisons across all 42 nodes. Absolute level of individual variation with respect to degree, betweenness, and participation coefficient was measured as the standard deviation across subjects. Variation in edge strength between two sulci was similarly assessed using unthresholded weighted networks.

Graph metrics were computed using the Python port (https://pypi.org/project/bctpy) of Brain Connectivity Toolbox (BCT). Statistics were computed using Python library statsmodels. For matrix visualization, nodes were ordered both by clusters and within each cluster to maximize the number of edges close to the main diagonal, using simulated annealing (BCT reorder_matrix). Visualizations were created using Matplotlib and NetworkX. Spring layout was generated using the Kamada-Kawai method.

Testing associations between sulcal depth and network centrality for three pTS in LPFC

Building on the previous finding that the depth of right pimfs, pmfs-a, and pmfs-i pTS (all assigned to the blue cluster) predicted reasoning performance beyond age (Voorhies et al., 2021), we tested whether the depth of these sulci also related to differences in functional organization during reasoning. First, we tested, for the left and right hemisphere counterpart

of each sulcus, whether its depth relates to its graph metrics (nodal degree, betweenness, and/or participation coefficient). Associations between depth and each metric were tested using ordinary least squares regression, controlling for age effects on depth and functional connectivity by including it as an additional explanatory variable (two-tailed tests, FDR-corrected across the 18 combinations of the six sulci and three graph metrics). We followed up with analogous regression analyses with individual edges as dependent variable to pinpoint the pairwise connections that drove the significant associations (one-tailed tests, FDR-corrected across the 42 connections investigated per sulcus).

Code accessibility

Scripts to perform data preprocessing and statistical analyses will be freely available with the publication of the paper on GitHub. Requests for further information or raw data should be directed to the corresponding authors.

Results

Sulci exhibited dissociable functional connectivity profiles

To assess whether (or which) sulci could be differentiated on the basis of their functional connectivity, we tested whether any two sulci for a given participant could be classified based on their connectivity fingerprints. Indeed, the SVM classifier could successfully discriminate each pair of sulci well above chance level (i.e., 50%) across participants, with very high accuracy for most – but not all – pairs of sulci (mean: 96%, range: 71–100%; FDR-corrected $p < 0.01$).

To assess whether correcting for spatial autocorrelations between neighboring sulci altered classification accuracy, we also ran the SVM analyses without correcting for them. Again here, classification accuracies were generally high (mean: 96%, range: 70–100%) –

albeit not quite as high ($t_{41} = 3.81$, $p < 0.001$). This higher accuracy with correction for autocorrelations was observed for the sulci that were closest together (< 5 mm geodesic distance) ($t_{971} = 2.43$, $p < 0.05$), as expected, and also for contralateral sulcal pairs ($t_{20} = 2.98$, $p < 0.01$). By contrast, there was no difference in the classification accuracy of sulcal pairs within one hemisphere at more than 10 mm apart ($t_{148} = 1.59$, $p > 0.1$). Overall, sulci across LPFC and LPC generally had differentiable connectivity profiles.

Functional clustering of LPFC and LPC sulci reveal within- and between-lobe sulcal networks

Next, we sought to test whether sulci clustered into groups with similar connectivity profiles. Group-level connectivity-based clustering of LPFC–LPC sulci repeated at 0.01–0.5 density thresholds (**Figure 2A**) revealed five major clusters of sulci (**Figure 2B**): one LPC (yellow), one LPFC (dark blue), and three clusters consisting of both LPFC and LPC sulci (red, green, purple). In addition, two sulci (slocs-v, cyan; cSTS3, medium blue) formed two distinct clusters with their interhemispheric counterparts at several thresholds. This analysis reveals, for the first time, sulcal-functional coupling both within and between LPFC and LPC sulci (**Figure 2B**).

Here, we highlight five key observations. First, LPFC pTS whose morphological features have been previously linked to individual differences in reasoning performance – right-hemisphere pimfs, pmfs-a, and pmfs-i (Voorhies et al., 2021), along with left pimfs (Willbrand et al., 2022, 2023b, 2024) clustered together (dark blue in **Figure 2B**). Second, several pTS in LPFC and LPC clustered together, despite being geographically distant (purple cluster). Third, inferior portions of the intraparietal sulcus (IPS-PO; yellow) clustered separately from more dorsal portions of the IPS (red in **Figure 2C**), which clustered with the inferior frontal sulcus (ifs). Fourth, the superior frontal sulcus (sfs) clustered with a subset of

branches of the superior temporal sulcus (STS) and pTS in inferior frontal cortex (green). Fifth, newly identified pTS in LPC (slocs-v) clustered by themselves (cyan in **Figure 2B**).

The sulci in these clusters also tended to be associated with different large-scale canonical resting-state networks (**Extended Data Figure 2-2**). While there was considerable individual variation between sulci in a cluster and across subjects, sulci within the red and purple clusters generally showed strongest correlations with the frontoparietal network and dorsal attention networks, green with the default mode network, and yellow with dorsal attention and visual networks. By contrast, sulci in the dark blue, cyan, and medium blue clusters were not clearly associated with any of these large-scale networks.

Co-clustering results suggested that clusters based on the group mean network generalized moderately well to individual participants (**Figure 2C**). Analyses in individual participants identified 5–10 clusters per participant (mean = 7), where each cluster was defined as including more than one sulcus and the cluster count was the maximum number identified across all clustering thresholds. Focusing on the clusters described above, capturing distinctions across thresholds (**Figure 2B**), the pairs of sulci within the same group-level cluster were assigned together at multiple thresholds in 80% of participants (yellow: 94%; medium blue: 91%; dark blue: 87%; purple: 86%; red: 73%, green: 76%; cyan: 70%;), which was higher than the 58% co-assignment for pairs that did not belong to the same group-level cluster ($t_{42} = 10.83$, two-tailed $p < 0.0001$). Thus, there was moderate agreement between individual and group-level cluster assignments, although there was also individual variability.

Importantly, the clustering patterns could not be explained by spatial autocorrelations among nearby sulci, for two main reasons. First, the preferential correlation among neighboring sulci in the LPFC pTS cluster (dark blue in **Figure 2C**) was observed despite being penalized via correction for spatial autocorrelations (see **Extended Data Figure 3-3** for all connectivity fingerprints with and without controlling for spatial autocorrelations).

Second, a number of geographically distant sulci clustered together (**Extended Data Figure 1-2**) – for example, the pmfs-p and the aipsJ (purple in **Figure 2C**) – demonstrating a novel functional connection between small, shallow sulci across LPFC and LPC.

Thus, a number of sulci both within and across LPFC and LPC had sufficiently similar patterns of functional connectivity that they were grouped together in the clustering analysis. Even though most sulcal pairs could be reliably dissociated by an SVM classifier, as noted previously, classifier performance tended to be lower – albeit still well above chance – for sulci assigned to the same group-level cluster (**Extended Data Figure 2-3**). With regards to individual variability in clustering, there was moderate agreement across participants in terms of which sulci were assigned to the same cluster (dark blue (LPFC) and purple (LPFC-LPC) pTS clusters (87% and 86% of participants, respectively) by comparison with the yellow and medium blue LPC clusters (94% and 91%).

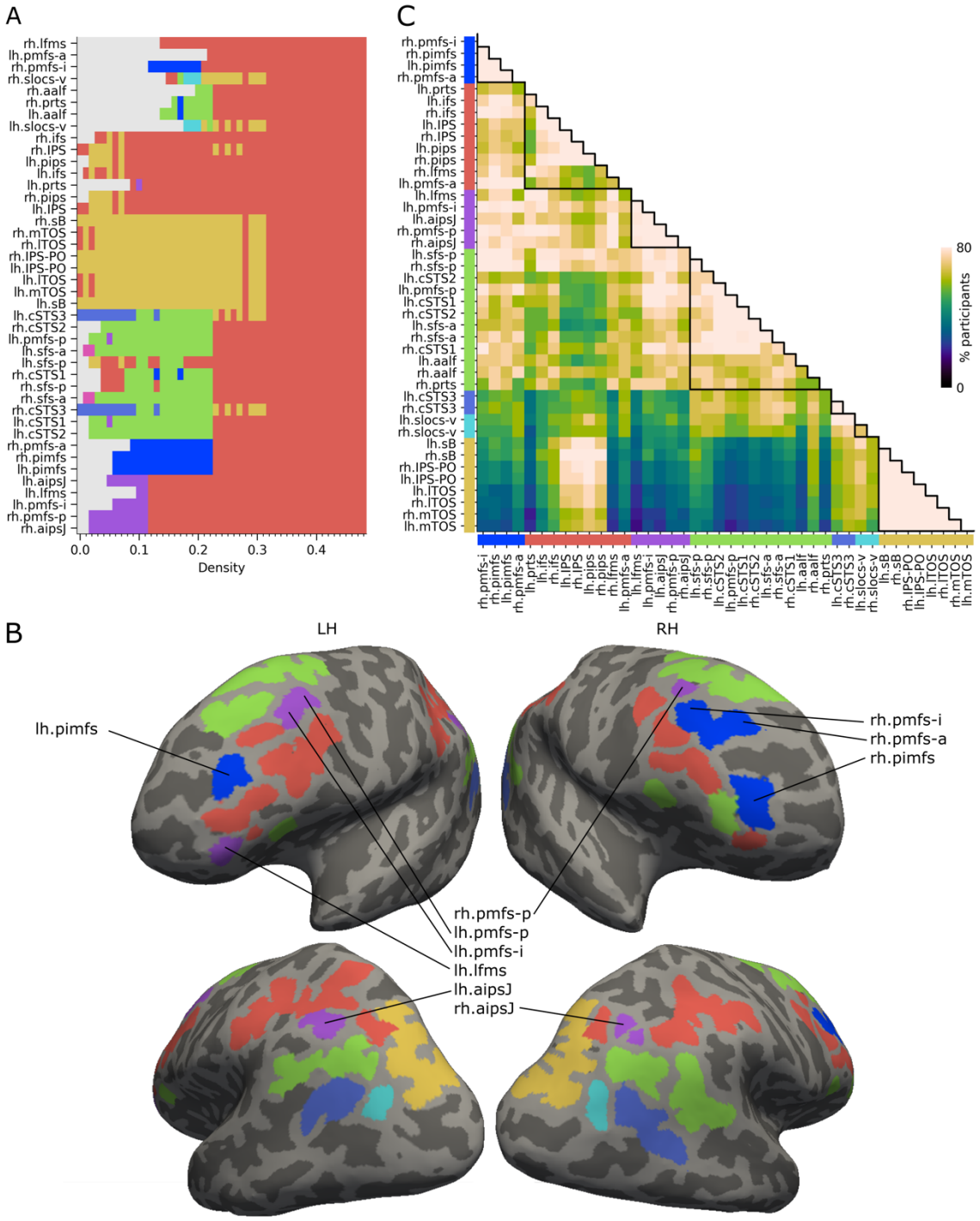

Figure 2. Lateral frontoparietal functional connectivity based on individual sulcal morphology. (A) Group average network (N = 43) clusters estimated at 0.01–0.5 density thresholds. Colors reflect cluster identity; white refers to nodes that are isolated or form a single-sulcus cluster at the threshold. (B) Clusters selected to capture distinctions across thresholds in the group results, displayed on the cortical surfaces of an example subject. The

colors correspond to those in panel A. The sulci assigned most consistently across thresholds to the dark blue and purple clusters, labeled here, consist only of pTS. The newly identified slocs-v (cyan) also clustered separately from other sulci. The other clusters included both large and deep, as well as small and shallow, sulci. (C) Co-clustering at the individual level in relation to the group-level results. This matrix displays the percentage of participants for whom any two sulci clustered together in individual-level clustering analyses. The sulci are grouped based on the group-level clustering results, as indicated by the colored bars along the axes. Lighter colors indicate sulcal pairs that clustered together at multiple thresholds for a larger number of participants. Pairs of sulci assigned to the same group-level cluster are delineated by black outlines; relatively strong agreement across participants is observed for these pairs. For results without correction for spatial autocorrelations, see **Extended Data Figure 2-1**. For associations of the clusters with canonical large-scale resting-state networks, see **Extended Data Figure 2-2**.

LPFC-LPC sulcal network topology and measures of centrality

We next looked more closely at the connectivity patterns of individual sulci. Perhaps unsurprisingly, sulci had on average strongest connections with other sulci that co-clustered with them based on overall connectivity profiles (**Figure 3A**, **B**; **Extended Data Figure 3-1**). To identify sulci with relatively high or low network connectivity, we compared measures of centrality for a given node to the average values across nodes for a given participant. We examined three measures of centrality: degree, betweenness, and participation coefficient (see Materials and Methods for descriptions).

Notably, almost all LPFC pTS scored below average with regards to at least one (and often more) centrality measure: bilateral pimfs, pmfs-a, and lfms, aalf, and prts, along with right pmfs-i (located in the dark blue, red, and green group-level clusters; **Figure 3C**). The only exceptions were found in the purple cluster. Right pmfs-p – along with bilateral aipsJ, a

pTS in LPC – scored above average in participation coefficient, with trend-level effects for the other centrality measures. Left pmfs-i showed average centrality values overall, but with relatively high variability in these metrics across participants (**Extended Data Figure 3-3**); this variability is explored below in relation to sulcal depth. These results were very similar when not controlling for spatial autocorrelations (**Extended Data Figure 3-2**). In sum, these results suggest that most LPFC pTS have relatively sparse connectivity; these results can be contrasted with LPC sulci IPS and IPS-PO, which scored consistently high in the centrality metrics across participants (each sulci $p < 0.05$, FDR corrected).

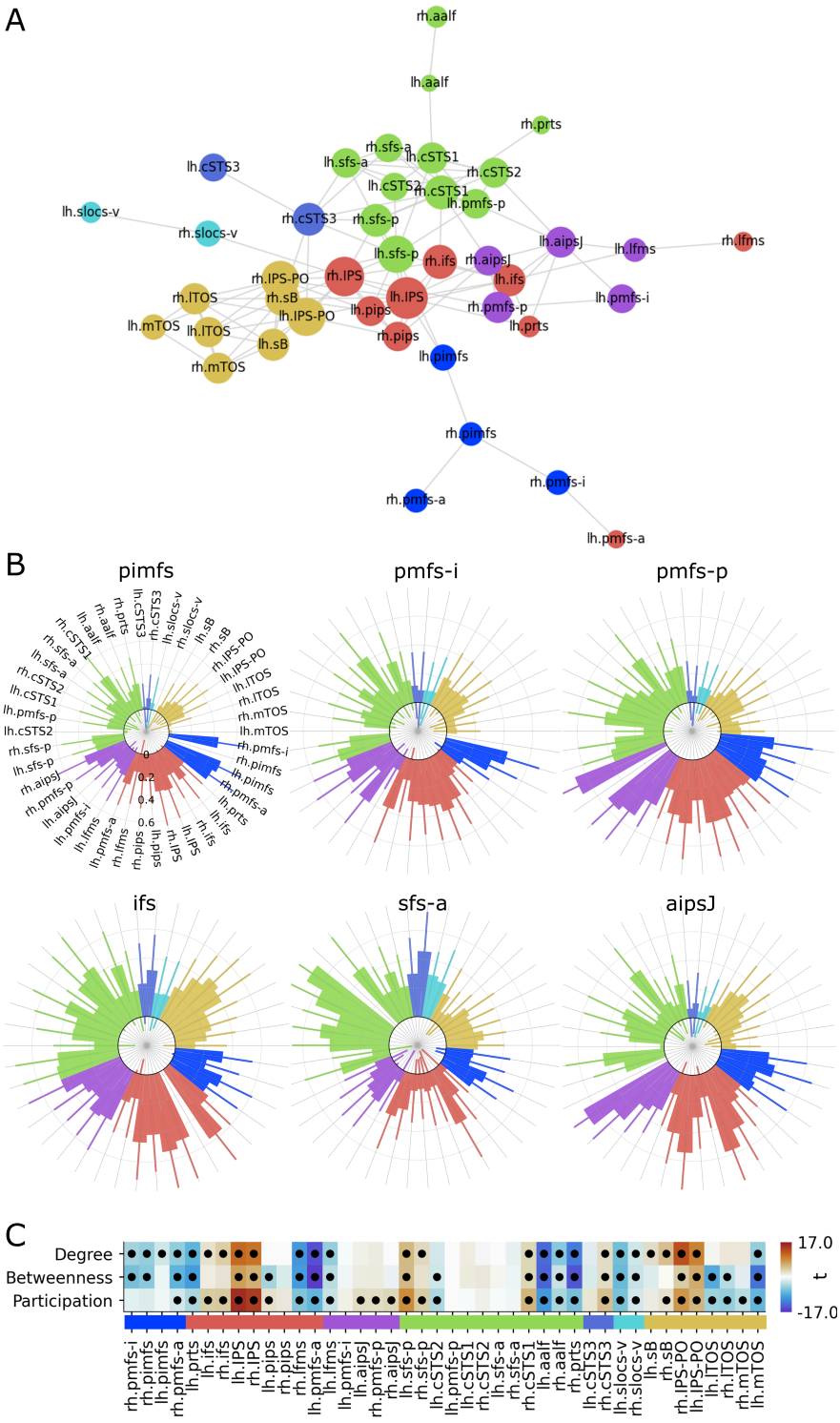

Figure 3. Functional organization of the sulcal LPFC–LPC network. (A) Spring plot of mean network, showing connections at 0.12 density and the strongest connection for the nodes isolated at this threshold. Each of the five larger clusters shows high connectivity within the cluster. Node size is proportional to mean AUC degree. (B) Functional

connectivity fingerprints (mean, SD) of selected right-hemisphere pTS in LPFC – pimfs and pmfs-i (dark blue cluster) and pmfs-p (purple cluster) — as well as adjacent larger sulci (ifs, sfs-a). The cluster colors match **Figure 2B**. (C) The nodes associated with significantly higher or lower centrality measures (degree, betweenness, and/or participation coefficient) relative to the mean of values of all nodes for a given participant. Cells are shaded according to strength of t-values for each comparison, with warm and cool colors denoting above and below mean. Black dots depict cells with significant (FDR-corrected $p < 0.05$) results when controlling for spatial autocorrelations. For pairwise connectivity analysis and anatomical illustration, see **Extended Data Figure 3-2**. For levels of individual variability, see **Extended Data Figure 3-3**.

Relationship between centrality and sulcal surface area

Observing that the graph analyses attributed higher centrality to large sulci such as those in IPS and IPS-PO than to small ones such as the pTS in the blue LPFC cluster, we explicitly tested whether functional connectedness was systematically related to sulcal surface area. To do so, we tested the relation between graph metrics and surface area with linear mixed effect models with random intercepts and slopes for participant and surface area, respectively. We did in fact observe a significant positive association with surface area for all three centrality measures (degree: $\beta = 0.59$, $p < 0.001$; betweenness: $\beta = 0.43$, $p < 0.001$; participation coefficient: $\beta = 0.58$, $p < 0.001$). This relationship could reflect a true feature of brain architecture and/or a methodological confound. (Given that the fMRI timeseries was averaged over all voxels in a sulcus, it is possible that sulci with a larger surface area had a higher signal-to-noise ratio than smaller ones, perhaps artificially boosting their centrality metrics). Either way, it is all the more meaningful that many of the small sulci have preferential connectivity to other small sulci rather than the larger ones.

Sulcal depth and functional connectivity are correlated for specific pTS in LPFC

We tested whether the functional connectivity patterns of right and/or left pimfs, pmfs-a, and pmfs-i sulci measured during performance of a reasoning task would be related to their depth, as we have previously found that the depths of these sulci in the right hemisphere was related to reasoning performance (Voorhies et al., 2021). We included age as a covariate to control for any possible spurious correlations related to age in both depth and functional connectivity. We found positive associations between depth and centrality measures for left pmfs-i, right pmfs-a, and left pimfs that survived correction for multiple comparisons (**Figure 4A**; **Extended Data Table 4-1**). These significant results were also obtained when not controlling for spatial autocorrelations.

We next investigated the spatial pattern of pairwise sulcal connections contributing to the positive depth-connectivity associations shown by graph measures. The edgewise regression analysis revealed that these effects were not driven by connectivity within the LPFC (dark blue) or LPFC-LPC (purple) pTS clusters (**Figure 4B**). Rather, associations between the depth of left pmfs-i and its connectivity were significant for both frontal (left sfs-p, left aalf) and parietal sulci (bilateral IPS, left IPS-PO, left lTOS, left sB; for scatter plots see **Extended Data Figure 4-1**). Individual edgewise associations for the depth of right pmfs-a did not reach significance, but at uncorrected thresholds the putative effects also involved both LPFC and LPC sulci. Taken together, these results indicate that left pmfs-i and right pmfs-a were more strongly connected across the LPFC–LPC sulcal network in participants in whom these sulci were deeper.

We also conducted exploratory analyses testing for sulcal depth-connectivity relationships for three additional pTS that have been largely overlooked in previous studies: 1) pmfs-p (in green/purple clusters in the left/right hemispheres), which does not cluster with other pmfs components and has not – unlike them – been linked to reasoning performance, 2)

aipsJ (in the LPFC-LPC purple cluster), a well-known pTS in LPC (Zlatkina and Petrides, 2014), and 3) slocs-v (small cyan cluster), a newly identified sulcus (Willbrand et al., 2023c) that was implicated with reasoning in a recent morphological study (Tsai et al., 2023). These exploratory analyses revealed significant depth–connectivity associations for bilateral aipsJ and right slocs-v (**Extended Data Figure 4-2**).

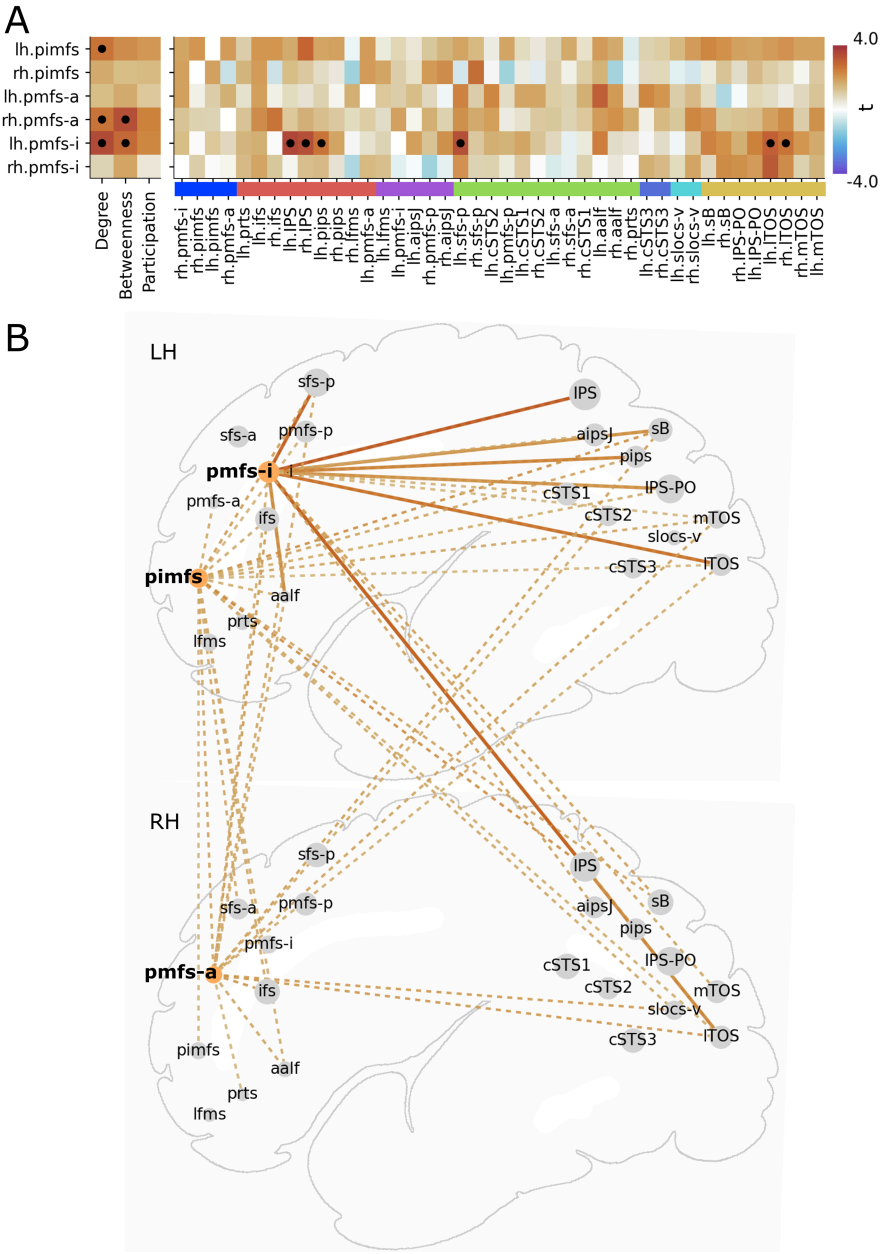

Figure 4. Sulcal depth and functional connectivity are correlated for specific pTS in LPFC. The depths of lh.pmfs-i, rh.pmfs-a, and left pimfs are positively correlated with their

functional connectivity, controlling for age in addition to spatial autocorrelations. (A) Left-most columns: results of regression analyses revealing significant associations between depth and centrality measures for lh.pmfs-i and rh.pmfs-a. Cells are shaded according to strength of t-values for each regression, with warm and cool colors denoting positive and negative correlations, and darker shades indicating higher values. Dots depict cells with significant result (FDR-corrected $p < 0.05$). Columns at right: correlations between the depth of each of these sulci and the strength of their pairwise functional connectivity with the other sulci. For statistical values both controlling and not controlling for age and spatial autocorrelations, see **Extended Data Table 4-1**. (B) Schematic illustrating the approximate anatomical distribution of sulci showing depth-related increases in pairwise connection strength (solid FDR-corrected, dashed trends at uncorrected $p < 0.05$). Node size reflects AUC estimate for degree. For scatterplots of significant effects, see **Extended Data Figure 4-1**.

Discussion

The present study characterized individual sulcal connectomes within and between LPFC and LPC in a data-driven manner. Classification analyses revealed that most sulci had characteristic functional connectivity profiles; nevertheless, they clustered into groups with similar connectivity profiles – and, in some cases, clustered with distant, rather than neighboring, sulci. We observed moderate agreement between group-level and individual-level cluster assignments, speaking to individual variability that is important to characterize. We report, for the first time, associations between individual variability in sulcal depth and graph metrics of functional connectivity. These findings add to the body of evidence that sulcal morphology is functionally relevant and provides network-level insight from the local sulcal anatomy that is specific to a given individual. Below, we discuss key observations, with an emphasis on the overlooked pTS.

Sulcal clustering according to functional connectivity profiles

Broadly, connectivity-based clustering revealed five major clusters of sulci at the group level that were stable across several clustering thresholds – along with two small clusters that each included only the left and right counterpart of a single sulcus. Two of the main group-level clusters included only pTS: an LPFC cluster (dark blue) and an LPFC-LPC cluster (purple), discussed below.

The LPFC cluster combines pimfs, pmfs-a, and pmfs-i – all LPFC pTS showing morphological associations with reasoning in previous studies (Voorhies et al., 2021; Willbrand et al., 2023a, 2023b). We observed strong local connectivity among these sulci and particularly weak connectivity between them and LPC sulci, consistent with local recurrent connectivity between these neighboring sulci in support of higher-level cognition. Of course, associations with other sulci also varied on an individual basis and at the group level. The LPC cluster includes left pmfs-i, right pmfs-p, and left lfms in LPFC and bilateral aipsJ in LPC. These sulci had similar connectivity profiles and showed strong functional connectivity with one another. Importantly, these results identify a new functional link between pTS in LPFC and LPC (aipsJ) that can motivate future work. This is clinically relevant, as the aipsJ is used as a corridor in neurosurgery to reach deeper structures, while minimizing damage to other structures (Tomaiuolo and Giordano, 2016; Tomaiuolo et al., 2022).

The sulcal-functional dissociations identified here are consistent with the handful of recent studies that have compared connectivity patterns of manually defined sulci in LPFC and LPC – albeit with a completely different approach. Unlike the present study, previous work first manually identified sulci in each cortical expanse and then calculated the overlap between resting state parcellations of the cerebral cortex in young adults from the Human Connectome Project that was conducted by a separate research group (Kong et al., 2019). Using this approach in LPFC, pmfs-a and pmfs-p were shown to be functionally distinct and

to overlap with different large-scale networks (Miller et al., 2021). Further, slocs-v, a newly identified pTS in LPC, overlapped with different networks compared to nearby larger surrounding sulci (Willbrand et al., 2023c). Additionally, a recent study in macaques demonstrated different clustering based on whole-brain functional connectivity for the putative homologs of pmfs-a and pmfs-i (Amiez et al., 2023). Integrating these parallel tracks of research and noting that pimfs, pmfs-a, pmfs-i, and pmfs-p are roughly positioned along a rostral-caudal axis, differences in their functional connectivity patterns may reflect the geographic location of the sulci within a larger anatomical and functional hierarchical gradient in LPFC (Miller, et al., 2021). Thus, further study is required to test the contributions of morphology vs. geographic location on the functional connectivity patterns of these LPFC sulci, as well as the roles of the small aipsJ (which clustered with LPFC pTS) and slocs-v (which clustered bilaterally by itself) in other LPFC-LPC networks in cognitive tasks beyond reasoning.

Network centrality is correlated with sulcal depth

Topologically, none of the pTS showed high centrality overall in the investigated sulcal LPFC–LPC network. From a network perspective, this is consistent with "preferential age attachment" theory, which suggests that early-developing nodes should become stronger hubs than those born later (Barabási and Albert, 1999) and has been recently suggested to apply in embryonic neurogenesis (Diez et al., 2022). The theory that the low overall centrality of pTS relate to their later development should be tested in a longitudinal sample in early childhood, while carefully controlling for the larger surface area of primary sulci.

Notably, although centrality was low on average for pTS, it was—for half of the sulci tested, both in our main analyses and exploratory ones—higher for individuals with deeper pTS. In a previous study (Voorhies et al., 2021), we showed that the depths of several right-hemisphere LPFC pTS (pimfs, pmfs-a, pmfs-i) were associated with reasoning performance.

Complementing this prior work, the depths of three of these six sulci (left pmfs-i, right pmfs-a, and left pimfs), were positively correlated with centrality measures, indicating stronger and more widespread connectivity. The specific pairwise connections implicated in these depth-connectivity associations included large and deep sulci in LPFC and LPC with high centrality measures (IPS, ifs, sfs-p) and sulci associated with the visual system (IPS-PO, lTOS), but not connectivity to neighboring sulci. Thus, greater depth was associated with stronger connectivity to geographically distant, larger, and presumably earlier developing sulci.

Given that we measured functional connectivity during performance of a reasoning task, we do not know whether the observed correlations with depth would be observed for 'intrinsic' connectivity measured with resting-state fMRI. Thus – although previous whole-brain connectivity studies generally describe relatively small effects of task-induced responses on global network organization (Cole et al., 2016; Gratton et al., 2018; Salvo et al., 2021) – it is unclear whether these depth correlations, as well as the sulcal clustering patterns and individual variability therein, are dependent on task state, which can be explored in future studies.

Future directions

The present results prompt further multi-modal characterization of pTS – including white matter measures, which may in some cases serve as a mechanistic link between cortical folding and functional brain architecture. Building on these results, important next steps will be to characterize short- and long-range white matter tracts between these sulci. In particular, the present findings beg the question of which LPFC and LPC pTS, if any, are directly connected via long-range white matter tracts. For example, the superior longitudinal fasciculus (SLF) is among the later-developing white matter bundles (Liang et al., 2022; Bagautdinova et al., 2023; Di Carlo et al., 2023). In particular, the middle branch of the SLF, connecting regions of the intraparietal sulcus to regions of the superior and middle frontal

gyrus – i.e. in the vicinity of the pmfs and aipsJ – is estimated to develop particularly late (Liang et al., 2022). This middle branch has also been proposed to provide anatomical communication between the dorsal and ventral attention systems for abstract processing far removed from perception and action (De Schotten et al., 2011; Parlatini et al., 2017; Suo et al., 2021), which resonates with the late development and morphological correlations of tertiary sulci reported previously.

Future research should also continue to explore the relationships between sulcal morphology and functional connectivity patterns. For example, prior studies have shown that sulcal variants are associated with differences in the organization of functional networks and task-related activation (Crosson, 1999; Amiez et al., 2013; Amiez and Petrides, 2014; Jahn et al., 2016; Lopez-Persem et al., 2019; Fedeli et al., 2020). We have previously found that the presence of the ventral pimfs in the left hemisphere was associated with reasoning performance in both pediatric and adult samples (Willbrand et al., 2022, 2024). While we showed here that the depth of left pimfs was correlated with a measure of network centrality, we combined the two branches of this sulcus for our present purposes (following Voorhies et al., 2021). Thus, exploring how functional connectivity differs in the presence or absence of left pimfs-v would serve as an effective testbed for continuing to explore the functional relevance of sulcal morphology.

Beyond functional architecture, the prolonged development of pTS anchors them to interesting questions about brain development in childhood and adolescence. Sulcal development during gestation has been theorized to serve as the foundation of functional architecture and cognition (Régis et al., 2005; Cachia et al., 2021; Weiner, 2023), and prenatal studies will be invaluable to test such fundamental principles and the stability of the sulcal-functional relationships across the decades of development. Additionally, pTS continue to exhibit changes after birth. For example, pmfs components were among LPFC

sulci showing most longitudinal thinning in 6–18 year-olds in prior work drawing on the same cohort as the present study (Willbrand et al., 2023b). These developments seem to coincide with increasing coupling of structural and functional measures (7–23 year-olds in Baum et al., 2020). Thus, future work could test longitudinal relationships between sulci, functional connectivity, and white matter microstructure over time within individuals. Further, measures associated with pTS may define a theoretically grounded starting point for exploring how early life experiences affect neurodevelopment and later cognitive outcomes.

References

Aichelburg C, Urbanski M, Thiebaut De Schotten M, Humbert F, Levy R, Volle E (2016) Morphometry of left frontal and temporal poles predicts analogical reasoning abilities. Cereb Cortex 26:915–932.

Amiez C, Neveu R, Warrot D, Petrides M, Knoblauch K, Procyk E (2013) The location of feedback-related activity in the midcingulate cortex is predicted by local morphology. J Neurosci 33:2217–2228.

Amiez C, Petrides M (2014) Neuroimaging evidence of the anatomo-functional organization of the human cingulate motor areas. Cereb Cortex 24:563–578.

Amiez C, Sallet J, Giacometti C, Verstraete C, Gandaux C, Morel-Latour V, Meguerditchian A, Hadj-Bouziane F, Ben Hamed S, Hopkins WD, Procyk E, Wilson CRE, Petrides M (2023) A revised perspective on the evolution of the lateral frontal cortex in primates. Sci Adv 9:eadf9445.

Bagautdinova J et al. (2023) Development of white matter fiber covariance networks supports executive function in youth. Cell Rep 42:113487.

Barabási A-L, Albert R (1999) Emergence of scaling in random networks. Science 286:509–512.

Baum GL, Cui Z, Roalf DR, Ciric R, Betzel RF, Larsen B, Cieslak M, Cook PA, Xia CH, Moore TM, Ruparel K, Oathes DJ, Alexander-Bloch AF, Shinohara RT, Raznahan A, Gur RE, Gur RC, Bassett DS, Satterthwaite TD (2020) Development of structure–function coupling in human brain networks during youth. Proc Natl Acad Sci 117:771–778.

Behzadi Y, Restom K, Liau J, Liu TT (2007) A component based noise correction method (CompCor) for BOLD and perfusion based fMRI. NeuroImage 37:90–101.

Benjamini Y, Hochberg Y (1995) Controlling the false discovery rate: a practical and powerful approach to multiple testing. J R Stat Soc Ser B Methodol 57:289–300.

Braga RM, Buckner RL (2017) Parallel interdigitated distributed networks within the individual estimated by intrinsic functional connectivity. Neuron 95:457-471.e5.

Cachia A, Borst G, Jardri R, Raznahan A, Murray GK, Mangin J-F, Plaze M (2021) Towards deciphering the fetal foundation of normal cognition and cognitive symptoms from sulcation of the cortex. Front Neuroanat 15:712862.

Cole MW, Ito T, Bassett DS, Schultz DH (2016) Activity flow over resting-state networks shapes cognitive task activations. Nat Neurosci 19:1718–1726.

Cox RW (1996) AFNI: Software for analysis and visualization of functional magnetic resonance neuroimages. Comput Biomed Res 29:162–173.

Crosson B (1999) Activity in the paracingulate and cingulate sulci during word generation: an fMRI study of functional anatomy. Cereb Cortex 9:307–316.

Dale AM, Fischl B, Sereno MI (1999) Cortical surface-based analysis: I. segmentation and surface reconstruction. NeuroImage 9:179–194.

De Schotten MT, Dell'Acqua F, Forkel SJ, Simmons A, Vergani F, Murphy DGM, Catani M (2011) A lateralized brain network for visuospatial attention. Nat Neurosci 14:1245–1246.

Destrieux C, Fischl B, Dale A, Halgren E (2010) Automatic parcellation of human cortical gyri and sulci using standard anatomical nomenclature. NeuroImage 53:1–15.

Di Carlo DT, Filice ME, Fava A, Quilici F, Fuochi B, Cecchi P, Donatelli G, Restani L, Nardini V, Turillazzi E, Cosottini M, Perrini P (2023) Development of associational fiber tracts in fetal human brain: a cadaveric laboratory investigation. Brain Struct Funct 228:2007–2015.

Diez I, Garcia-Moreno F, Carral-Sainz N, Stramaglia S, Nieto-Reyes A, D'Amato M, Cortes JM, Bonifazi P (2022) Linking hubness, embryonic neurogenesis, transcriptomics and diseases in human brain networks. bioRxiv 2022.04.01.486541. https://doi.org/10.1101/2022.04.01.486541

Dixon ML, De La Vega A, Mills C, Andrews-Hanna J, Spreng RN, Cole MW, Christoff K (2018) Heterogeneity within the frontoparietal control network and its relationship to the default and dorsal attention networks. Proc Natl Acad Sci 115.

Duncan J, Assem M, Shashidhara S (2020) Integrated intelligence from distributed brain activity. Trends Cogn Sci 24:838–852.

Esteban O, Birman D, Schaer M, Koyejo OO, Poldrack RA, Gorgolewski KJ (2017) MRIQC: Advancing the automatic prediction of image quality in MRI from unseen sites. PLOS ONE 12:e0184661.

Esteban O, Markiewicz CJ, Blair RW, Moodie CA, Isik AI, Erramuzpe A, Kent JD, Goncalves M, DuPre E, Snyder M, Oya H, Ghosh SS, Wright J, Durnez J, Poldrack RA, Gorgolewski KJ (2019) fMRIPrep: a robust preprocessing pipeline for functional MRI. Nat Methods 16:111–116.

Fedeli D, Del Maschio N, Caprioglio C, Sulpizio S, Abutalebi J (2020) Sulcal pattern variability and dorsal anterior cingulate cortex functional connectivity across adult age. Brain Connect 10:267–278.

Fischl B (2004) Automatically parcellating the human cerebral cortex. Cereb Cortex 14:11–22.

Fischl B, Dale AM (2000) Measuring the thickness of the human cerebral cortex from magnetic resonance images. Proc Natl Acad Sci 97:11050–11055.

Friston KJ, Williams S, Howard R, Frackowiak RSJ, Turner R (1996) Movement-related effects in fMRI time-series: movement artifacts in fMRI. Magn Reson Med 35:346–355.

Galar M, Fernández A, Barrenechea E, Bustince H, Herrera F (2011) An overview of ensemble methods for binary classifiers in multi-class problems: Experimental study on one-vs-one and one-vs-all schemes. Pattern Recognit 44:1761–1776.

Gilmore AW, Nelson SM, McDermott KB (2021) Precision functional mapping of human memory systems. Curr Opin Behav Sci 40:52–57.

Gordon EM et al. (2017) Precision functional mapping of individual human brains. Neuron 95:791–807.e7.

Gordon EM, Laumann TO, Marek S, Raut RV, Gratton C, Newbold DJ, Greene DJ, Coalson RS, Snyder AZ, Schlaggar BL, Petersen SE, Dosenbach NUF, Nelson SM (2020) Default-mode network streams for coupling to language and control systems. Proc Natl Acad Sci 117:17308–17319.

Gordon EM, Nelson SM (2021) Three types of individual variation in brain networks revealed by single-subject functional connectivity analyses. Curr Opin Behav Sci 40:79–86.

Gorgolewski K, Burns CD, Madison C, Clark D, Halchenko YO, Waskom ML, Ghosh SS (2011) Nipype: a flexible, lightweight and extensible neuroimaging data processing framework in Python. Front Neuroinformatics 5.

Gratton C, Laumann TO, Nielsen AN, Greene DJ, Gordon EM, Gilmore AW, Nelson SM, Coalson RS, Snyder AZ, Schlaggar BL, Dosenbach NUF, Petersen SE (2018) Functional brain networks are dominated by stable group and individual factors, not cognitive or daily variation. Neuron 98:439–452.e5.

Greve DN, Fischl B (2009) Accurate and robust brain image alignment using boundary-based registration. NeuroImage 48:63–72.

Hermosillo RJM et al. (2024) A precision functional atlas of personalized network topography and probabilities. Nat Neurosci. https://doi.org/10.1038/s41593-024-01596-5

Jahn A, Nee DE, Alexander WH, Brown JW (2016) Distinct regions within medial prefrontal cortex process pain and cognition. J Neurosci 36:12385–12392.

Jenkinson M, Bannister P, Brady M, Smith S (2002) Improved optimization for the robust and accurate linear registration and motion correction of brain images. NeuroImage 17:825–841.

Jung RE, Haier RJ (2007) The parieto-frontal integration theory (P-FIT) of intelligence: converging neuroimaging evidence. Behav Brain Sci 30:135–154.

Klein A, Ghosh SS, Bao FS, Giard J, Häme Y, Stavsky E, Lee N, Rossa B, Reuter M, Chaibub Neto E, Keshavan A (2017) Mindboggling morphometry of human brains. PLOS Comput Biol 13:e1005350.

Kong R, Li J, Orban C, Sabuncu MR, Liu H, Schaefer A, Sun N, Zuo X-N, Holmes AJ, Eickhoff SB, Yeo BTT (2019) Spatial topography of individual-specific cortical networks predicts human cognition, personality, and emotion. Cereb Cortex 29:2533–2551.

Krawczyk DC, Michelle McClelland M, Donovan CM (2011) A hierarchy for relational reasoning in the prefrontal cortex. Cortex 47:588–597.

Liang W, Yu Q, Wang W, Dhollander T, Suluba E, Li Z, Xu F, Hu Y, Tang Y, Liu S (2022) A comparative study of the superior longitudinal fasciculus subdivisions between neonates and young adults. Brain Struct Funct 227:2713–2730.

Lopez-Persem A, Verhagen L, Amiez C, Petrides M, Sallet J (2019) The human ventromedial prefrontal cortex: sulcal morphology and its influence on functional organization. J Neurosci 39:3627–3639.

Luria AR (1966) *Higher cortical functions in man*. New York: Springer.

Miller JA, Voorhies WI, Lurie DJ, D'Esposito M, Weiner KS (2021) Overlooked tertiary sulci serve as a meso-scale link between microstructural and functional properties of human lateral prefrontal cortex. J Neurosci 41:2229–2244.

Murphy AC, Bertolero MA, Papadopoulos L, Lydon-Staley DM, Bassett DS (2020) Multimodal network dynamics underpinning working memory. Nat Commun 11:3035.

Parlatini V, Radua J, Dell'Acqua F, Leslie A, Simmons A, Murphy DG, Catani M, Thiebaut De Schotten M (2017) Functional segregation and integration within fronto-parietal networks. NeuroImage 146:367–375.

Petrides M (2019) *Atlas of the Morphology of the Human Cerebral Cortex on the Average MNI Brain.* Academic Press.

Power JD, Mitra A, Laumann TO, Snyder AZ, Schlaggar BL, Petersen SE (2014) Methods to detect, characterize, and remove motion artifact in resting state fMRI. NeuroImage 84:320–341.

Régis J, Mangin J-F, Ochiai T, Frouin V, Riviére D, Cachia A, Tamura M, Samson Y (2005) "Sulcal root" generic model: a hypothesis to overcome the variability of the human cortex folding patterns. Neurol Med Chir (Tokyo) 45:1–17.

Roca M, Parr A, Thompson R, Woolgar A, Torralva T, Antoun N, Manes F, Duncan J (2010) Executive function and fluid intelligence after frontal lobe lesions. Brain 133:234–247.

Rosvall M, Bergstrom CT (2008) Maps of random walks on complex networks reveal community structure. Proc Natl Acad Sci 105:1118–1123.

Rubinov M, Sporns O (2010) Complex network measures of brain connectivity: Uses and interpretations. NeuroImage 52:1059–1069.

Salvo JJ, Holubecki AM, Braga RM (2021) Correspondence between functional connectivity and task-related activity patterns within the individual. Curr Opin Behav Sci 40:178–188.

Seitzman BA, Gratton C, Laumann TO, Gordon EM, Adeyemo B, Dworetsky A, Kraus BT, Gilmore AW, Berg JJ, Ortega M, Nguyen A, Greene DJ, McDermott KB, Nelson SM, Lessov-Schlaggar CN, Schlaggar BL, Dosenbach NUF, Petersen SE (2019) Trait-like variants in human functional brain networks. Proc Natl Acad Sci 116:22851–22861.

Shinn M, Hu A, Turner L, Noble S, Preller KH, Ji JL, Moujaes F, Achard S, Scheinost D, Constable RT, Krystal JH, Vollenweider FX, Lee D, Anticevic A, Bullmore ET, Murray JD (2023) Functional brain networks reflect spatial and temporal autocorrelation. Nat Neurosci 26:867–878.

Smith DM, Perez DC, Porter A, Dworetsky A, Gratton C (2021) Light through the fog: using precision fMRI data to disentangle the neural substrates of cognitive control. Curr Opin Behav Sci 40:19–26.

Stuss DT, Knight RT (2013) Principles of frontal lobe function. Oxford University Press, USA.

Suo X, Ding H, Li X, Zhang Y, Liang M, Zhang Y, Yu C, Qin W (2021) Anatomical and functional coupling between the dorsal and ventral attention networks. NeuroImage 232:117868.

Tomaiuolo F, Giordano F (2016) Cerebal sulci and gyri are intrinsic landmarks for brain navigation in individual subjects: an instrument to assist neurosurgeons in preserving cognitive function in brain tumour surgery (Commentary on Zlatkina *et al* .). Eur J Neurosci 43:1266–1267.

Tomaiuolo F, Raffa G, Morelli A, Rizzo V, Germanó A, Petrides M (2022) Sulci and gyri are topological cerebral landmarks in individual subjects: a study of brain navigation during tumour resection. Eur J Neurosci 55:2037–2046.

Tsai Y-HR, Willbrand EH, Voorhies WI, Gagnant T, Bunge SA, Weiner KS (2023) Linking reasoning performance during development to sulcal depth in lateral parietal cortex (LPC) & lateral parieto-occipital junction (LPOJ). Poster Present Flux Int Congr Dev Cogn Neurosci 2023 Sept 6-9 St Rosa CA USA.

Tustison NJ, Avants BB, Cook PA, Yuanjie Zheng, Egan A, Yushkevich PA, Gee JC (2010) N4ITK: Improved N3 Bias Correction. IEEE Trans Med Imaging 29:1310–1320.

Voorhies WI, Miller JA, Yao JK, Bunge SA, Weiner KS (2021) Cognitive insights from tertiary sulci in prefrontal cortex. Nat Commun 12:5122.

Wandell BA, Chial S, Backus BT (2000) Visualization and measurement of the cortical surface. J Cogn Neurosci 12:739–752.

Wechsler D (1949) *Wechsler Intelligence Scale for Children–Fourth Edition (WISC-IV).* The Psychological Corporation.

Weiner KS (2023) The hypothesis of fundal cognition. Nat Rev Neurosci 24:521–521.

Weiner KS, Natu VS, Grill-Spector K (2018) On object selectivity and the anatomy of the human fusiform gyrus. NeuroImage 173:604–609.

Wendelken C, Ferrer E, Whitaker KJ, Bunge SA (2016) Fronto-parietal network reconfiguration supports the development of reasoning ability. Cereb Cortex 26:2178–2190.

Wendelken C, O'Hare ED, Whitaker KJ, Ferrer E, Bunge SA (2011) Increased functional selectivity over development in rostrolateral prefrontal cortex. J Neurosci 31:17260–17268.

Willbrand EH, Bunge SA, Weiner KS (2023a) Neuroanatomical and functional dissociations between variably present anterior lateral prefrontal sulci. J Cogn Neurosci 35:1846–1867.

Willbrand EH, Ferrer E, Bunge SA, Weiner KS (2023b) Development of human lateral prefrontal sulcal morphology and its relation to reasoning performance. J Neurosci 43:2552–2567.

Willbrand EH, Jackson S, Chen S, Hathaway CB, Voorhies WI, Bunge SA, Weiner KS (2024) Cognitive relevance of an evolutionarily new and variable prefrontal structure. Brain Struct Funct 229:387–402.

Willbrand EH, Tsai Y-H, Gagnant T, Weiner KS (2023c) Updating the sulcal landscape of the human lateral parieto-occipital junction provides anatomical, functional, and cognitive insights. eLife 12:RP90451.

Willbrand EH, Voorhies WI, Yao JK, Weiner KS, Bunge SA (2022) Presence or absence of a prefrontal sulcus is linked to reasoning performance during child development. Brain Struct Funct 227:2543–2551.

Woolgar A, Parr A, Cusack R, Thompson R, Nimmo-Smith I, Torralva T, Roca M, Antoun N, Manes F, Duncan J (2010) Fluid intelligence loss linked to restricted regions of damage within frontal and parietal cortex. Proc Natl Acad Sci 107:14899–14902.

Yao JK, Voorhies WI, Miller JA, Bunge SA, Weiner KS (2023) Sulcal depth in prefrontal cortex: A novel predictor of working memory performance. Cereb Cortex 33:1799–1813.

Yeo BTT, Krienen FM, Sepulcre J, Sabuncu MR, Lashkari D, Hollinshead M, Roffman JL, Smoller JW, Zöllei L, Polimeni JR, Fischl B, Liu H, Buckner RL (2011) The organization of the human cerebral cortex estimated by intrinsic functional connectivity. J Neurophysiol 106:1125–1165.

Zhang Y, Brady M, Smith S (2001) Segmentation of brain MR images through a hidden Markov random field model and the expectation-maximization algorithm. IEEE Trans Med Imaging 20:45–57.

Zlatkina V, Petrides M (2014) Morphological patterns of the intraparietal sulcus and the anterior intermediate parietal sulcus of Jensen in the human brain. Proc R Soc B Biol Sci 281:20141493.

Extended Data

Extended Data Table 1-1. Summary of participant demographics. Parent/Guardian reported Family income, Education, Race, and Ethnicity.

Annual Household Income	Count
$16,000 to $24,999	2
$25,000 to $34,000	2
$35,000 to $49,999	1
$50,000 to $74,999	3
$75,000 to $99,999	6
Over $100,000	15
Over $200,000	3
Unknown/Not Reported	11
Highest Degree Earned by Parent/Guardian	
High School/GED	6
Associate degree	3
Bachelor's degree	13
Master's degree	9
Doctorate	1
Professional	4
Other	1
Unknown/Not Reported	6
Ethnic Categories	
Hispanic or Latino	1
Not Hispanic or Latino	21
Unknown/Not Reported	21
Racial Categories	

American Indian/Alaskan Native	0
Asian	2
Black or African American	7
Native Hawaiian or Other Pacific Islander	0
White	20
More Than One Race	12
Unknown/Not Reported	2

Extended Data Figure 1-1. Sulcal definitions in all participants. Colors and sulcal names match **Figure 1A**.

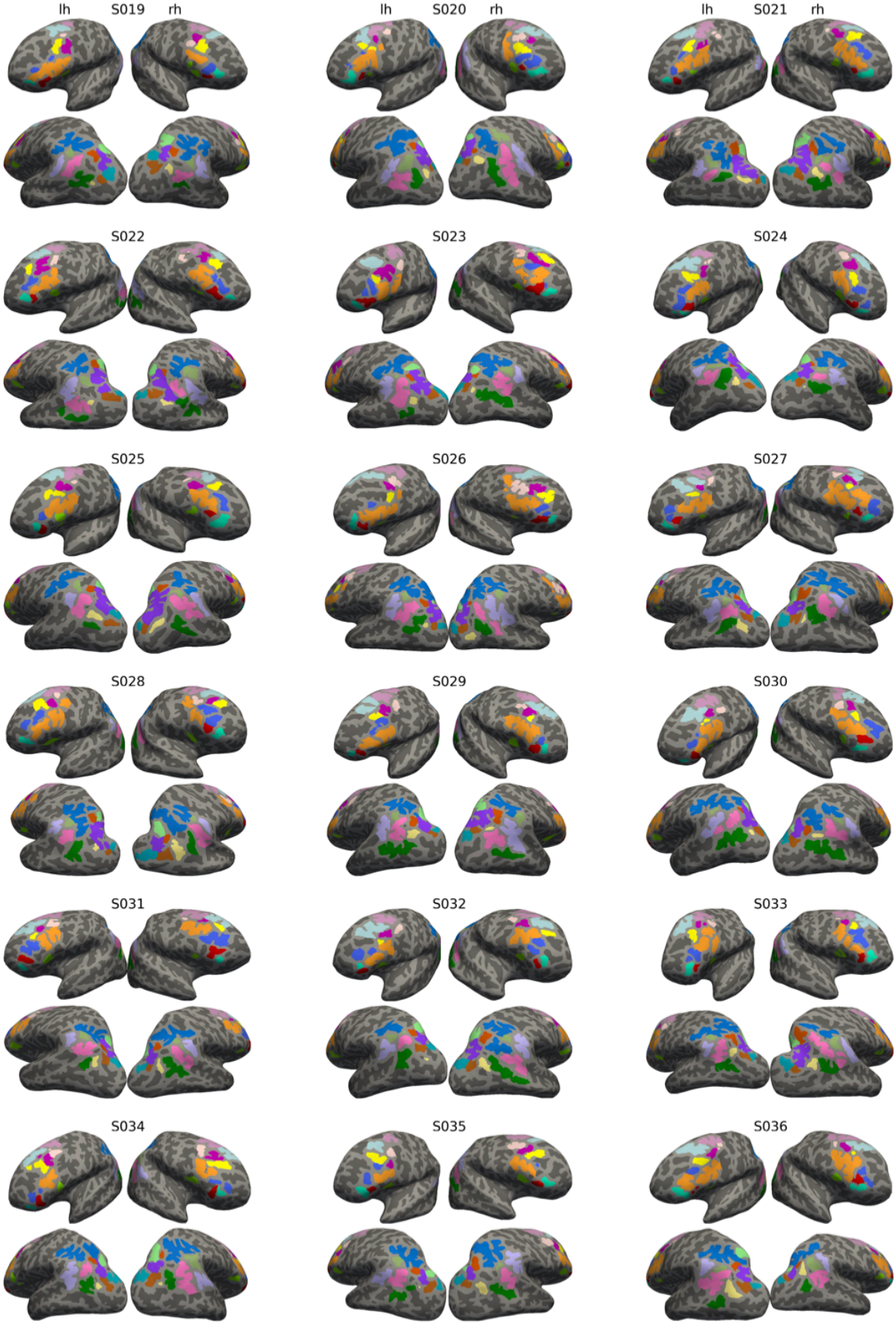
lh
S019
rh
lh
S020
rh
lh
S021
rh
S022
S023
S024
S025
S026
S027
S028
S029
S030
S031
S032
S033
S034
S035
S036

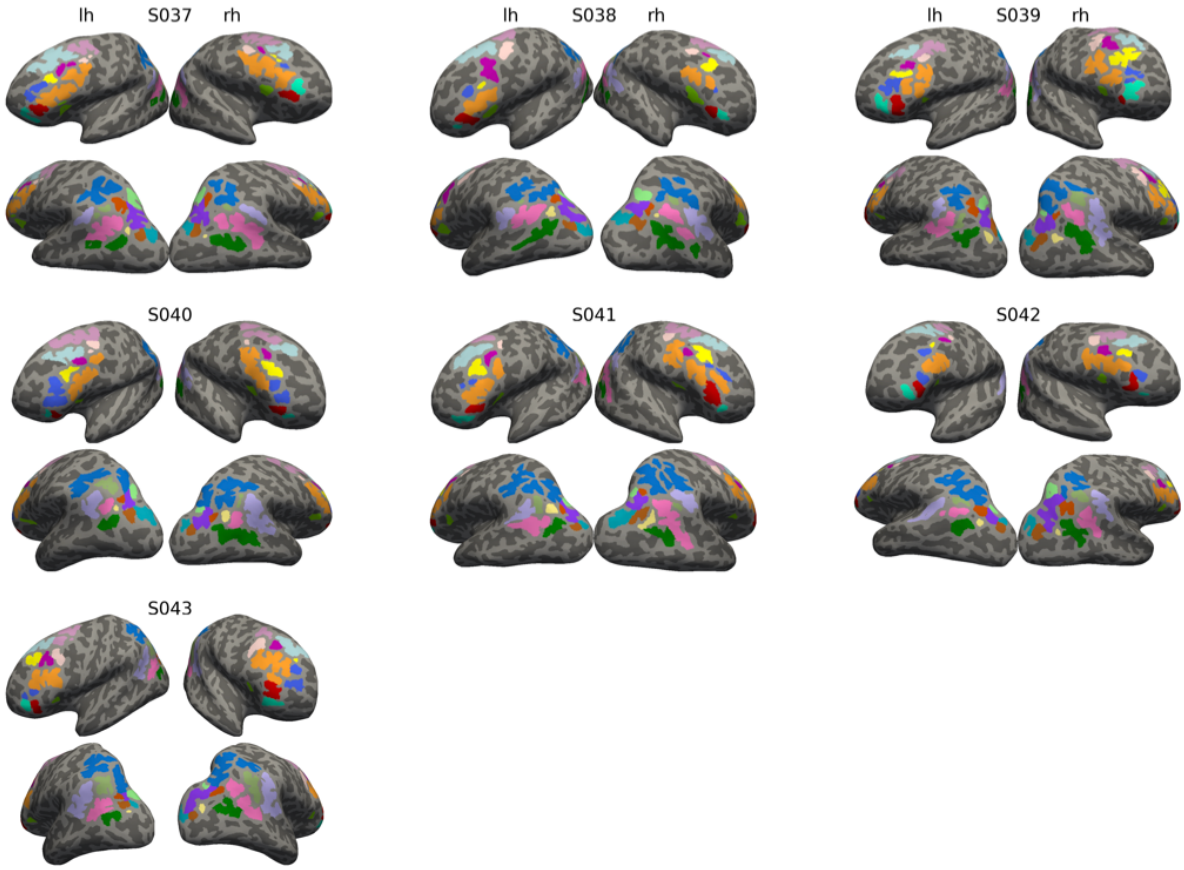
lh
S037
rh
lh
S038
rh
lh
S039
rh
S040
S041
S042
S043

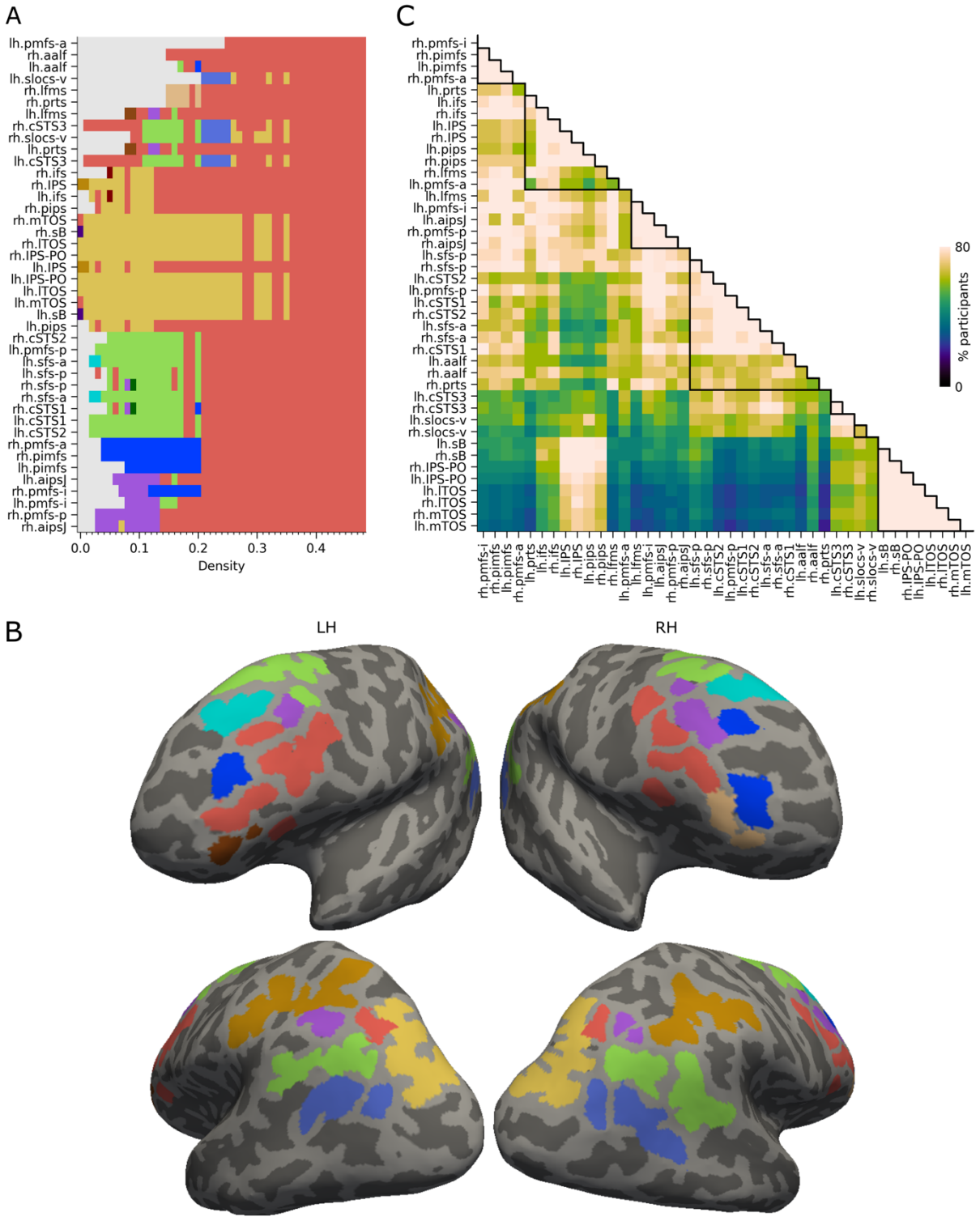

Extended Data Figure 2-1. Functional clustering of LPFC and LPC sulci without controlling for spatial autocorrelations. (A) Group average network (N = 43) clusters estimated at 0.01–0.5 density thresholds. Colors reflect cluster identity, and white refers to isolated nodes –i.e., nodes that form a single-sulcus cluster at a given threshold.

(B) Anatomical correspondence of composite clustering (showing all distinctions present at several thresholds in group results), analogous to the main analysis, on cortical surfaces of an example subject. Colors in panel (B) match those in panel (A). There are a number of similarities to the clustering in **Figure 2C**, although some clusters have broken apart and others have merged, (C) Individual-level assessment of the occurrence of clusters in individual-level clustering results. Lighter colors indicate sulcal pairs that frequency clustered together across subjects. The sulci are ordered as in **Figure 2C** for ease of comparison.

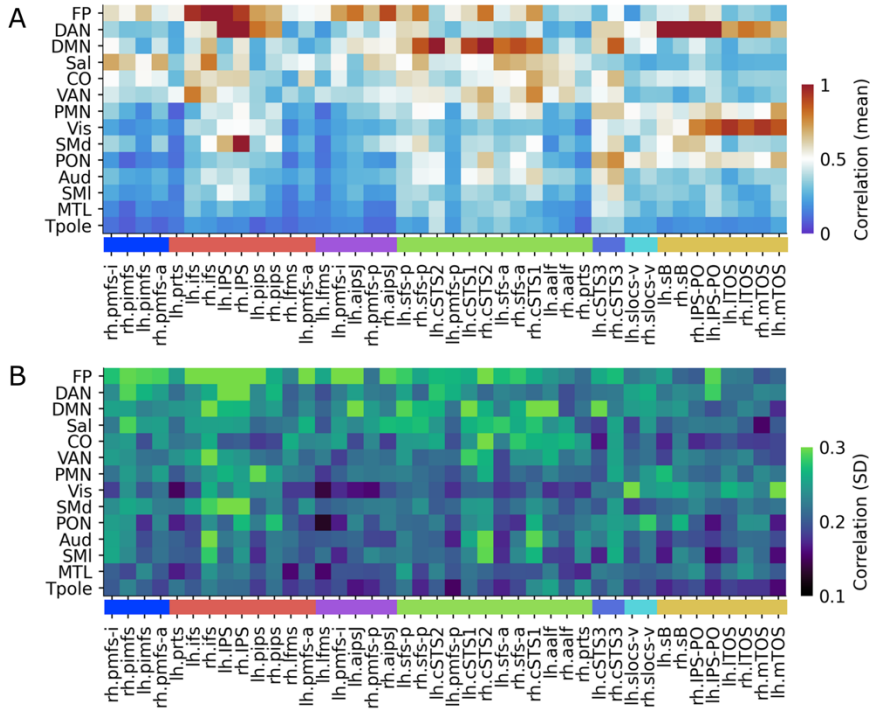

Extended Data Figure 2-2. Associations of LPFC and LPC sulci with canonical large-scale resting-state fMRI networks. The mean (A; N = 43) and individual variability (B) across individuals of the correlation in the timeseries of each sulcal and network mask area. FP: frontal parietal network; DAN: dorsal attention network; DMN: default mode network; Sal: salience network; CO: cingulo-opercular network; VAN: ventral attention network; PMN: parietal medial network; Vis: visual network; SMd: sensorimotor dorsal network;

PON: parieto-occipital network; Aud: auditory network; SMl sensorimotor lateral network; MTL: medial temporal network; Tpole: temporal pole network.

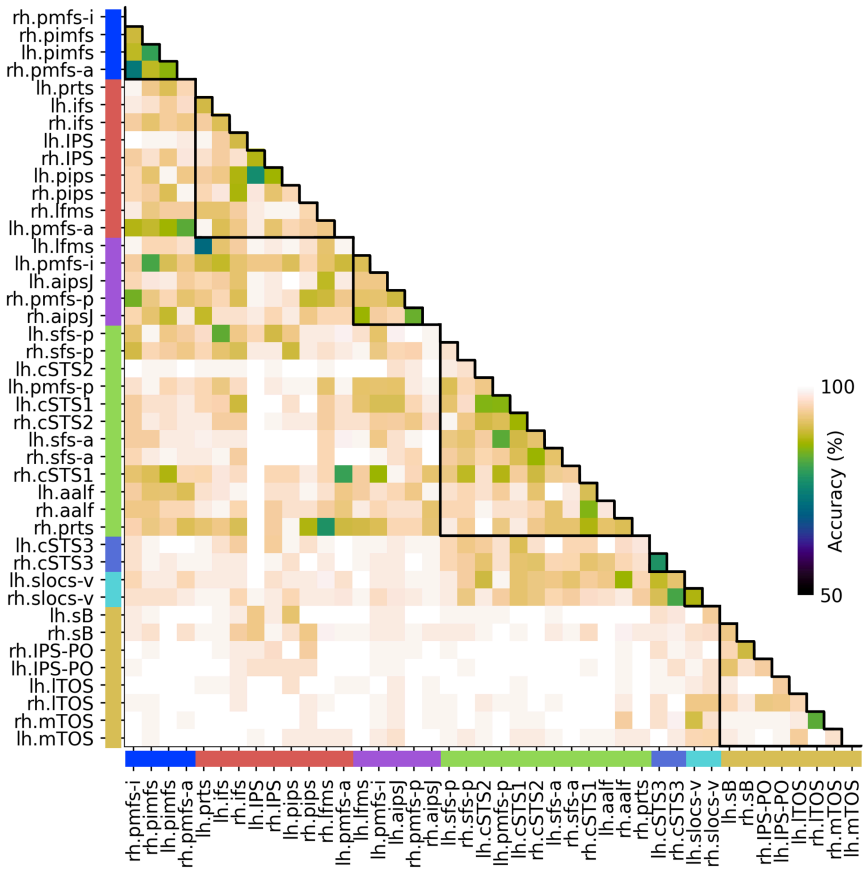

Extended Data Figure 2-3. Discriminability of pairs of sulci both within and between clusters, based on SVM classification of functional connectivity profiles. Cells are shaded according to pairwise classification accuracy, with lighter colors denoting better discriminability based on functional connectivity. All sulcal pairs showed cross-validated accuracy well over chance level (50%), confirmed by permutation testing (FDR-corrected $p < 0.01$). Black lines delineate pairs of sulci assigned to the same group-level cluster; discriminability between these sulci is expected to be lower than for sulci from different clusters, based on how the clusters were defined, but was still well above chance.

Extended Data Figure 3-1. Functional connectivity fingerprints with and without correction for spatial autocorrelations. The colors match the clusters in **Figure 2B**.

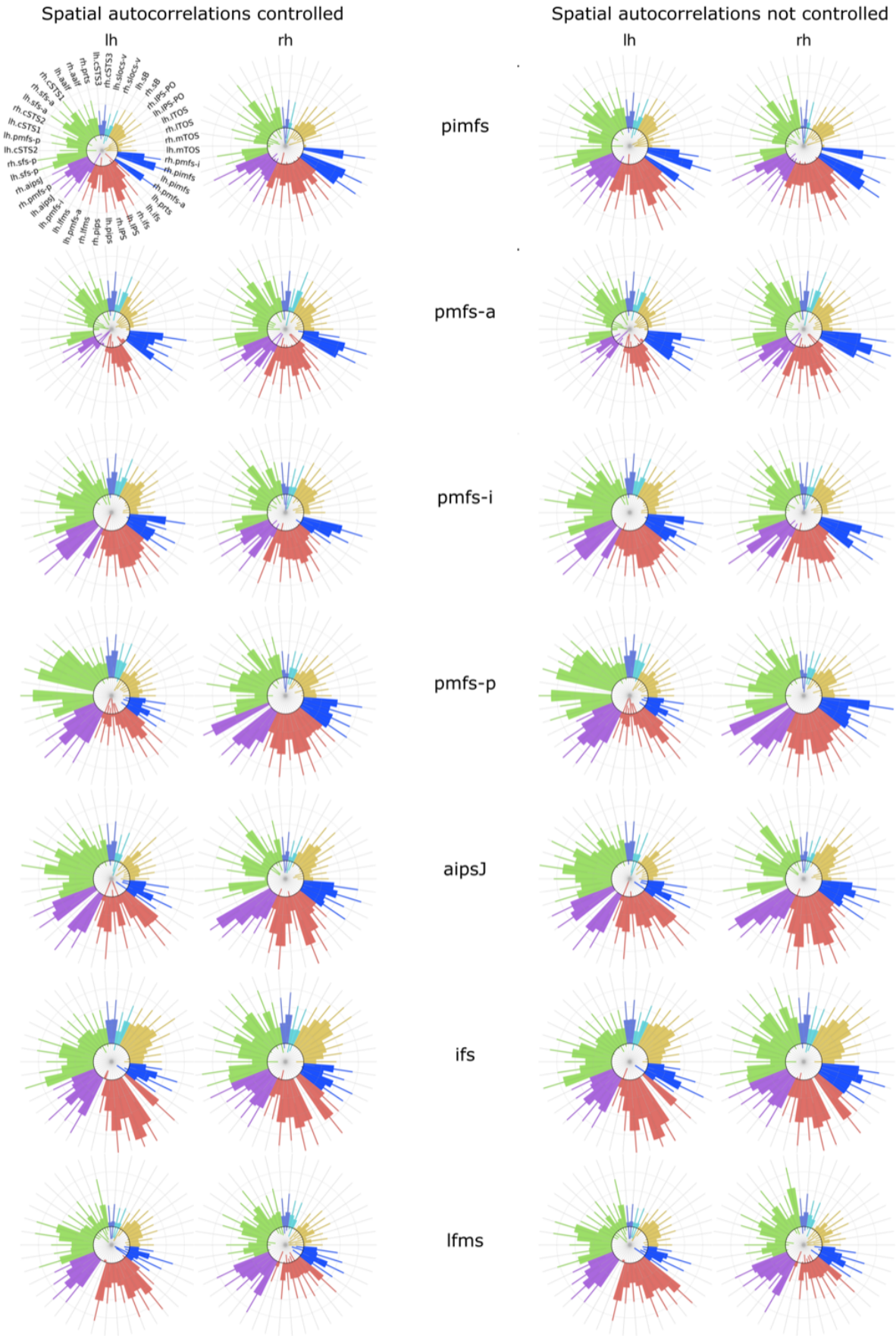

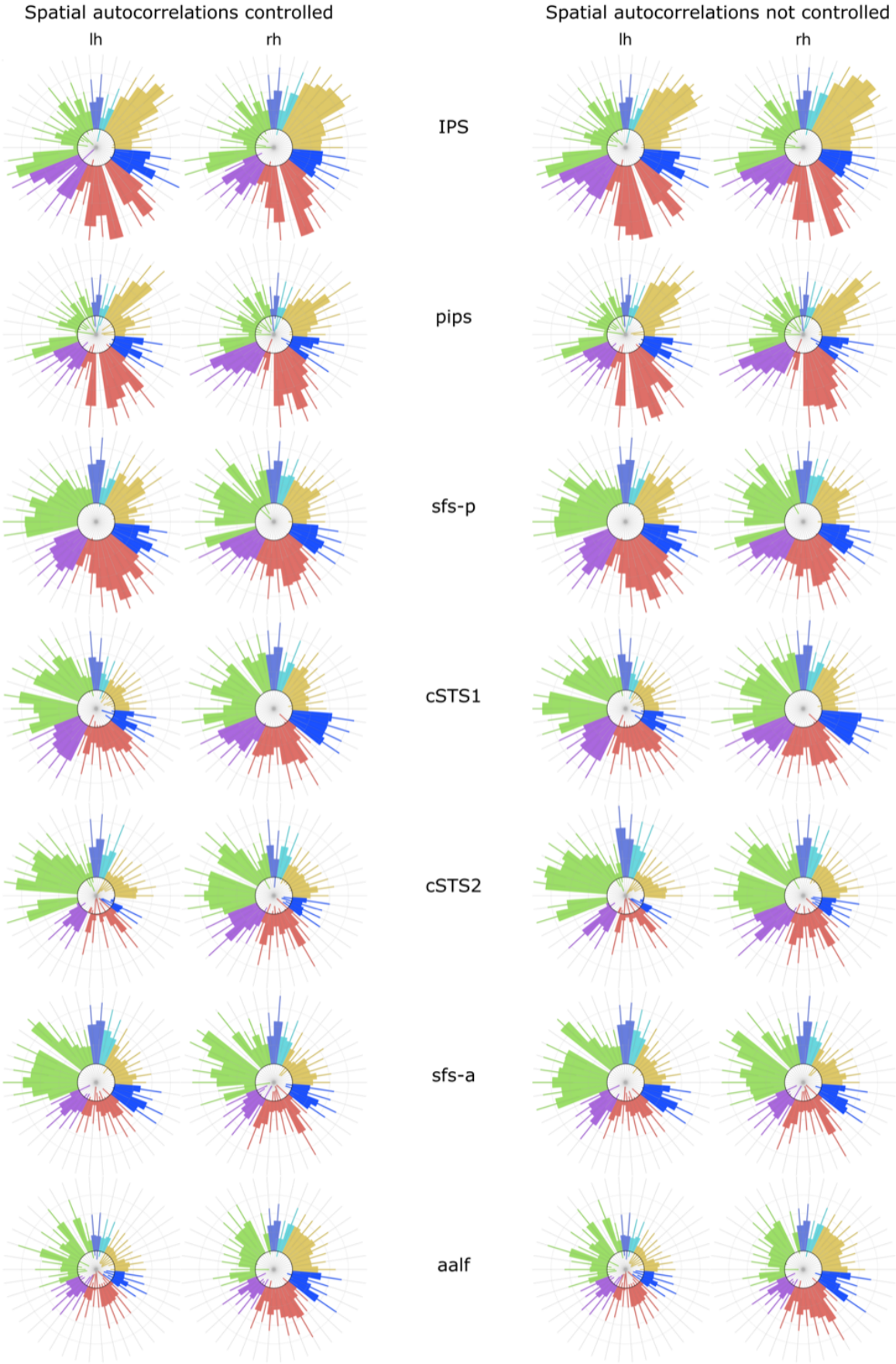
Spatial autocorrelations controlled
lh
rh
Spatial autocorrelations not controlled
lh
rh
IPS
pips
sfs-p
cSTS1
cSTS2
sfs-a
aalf

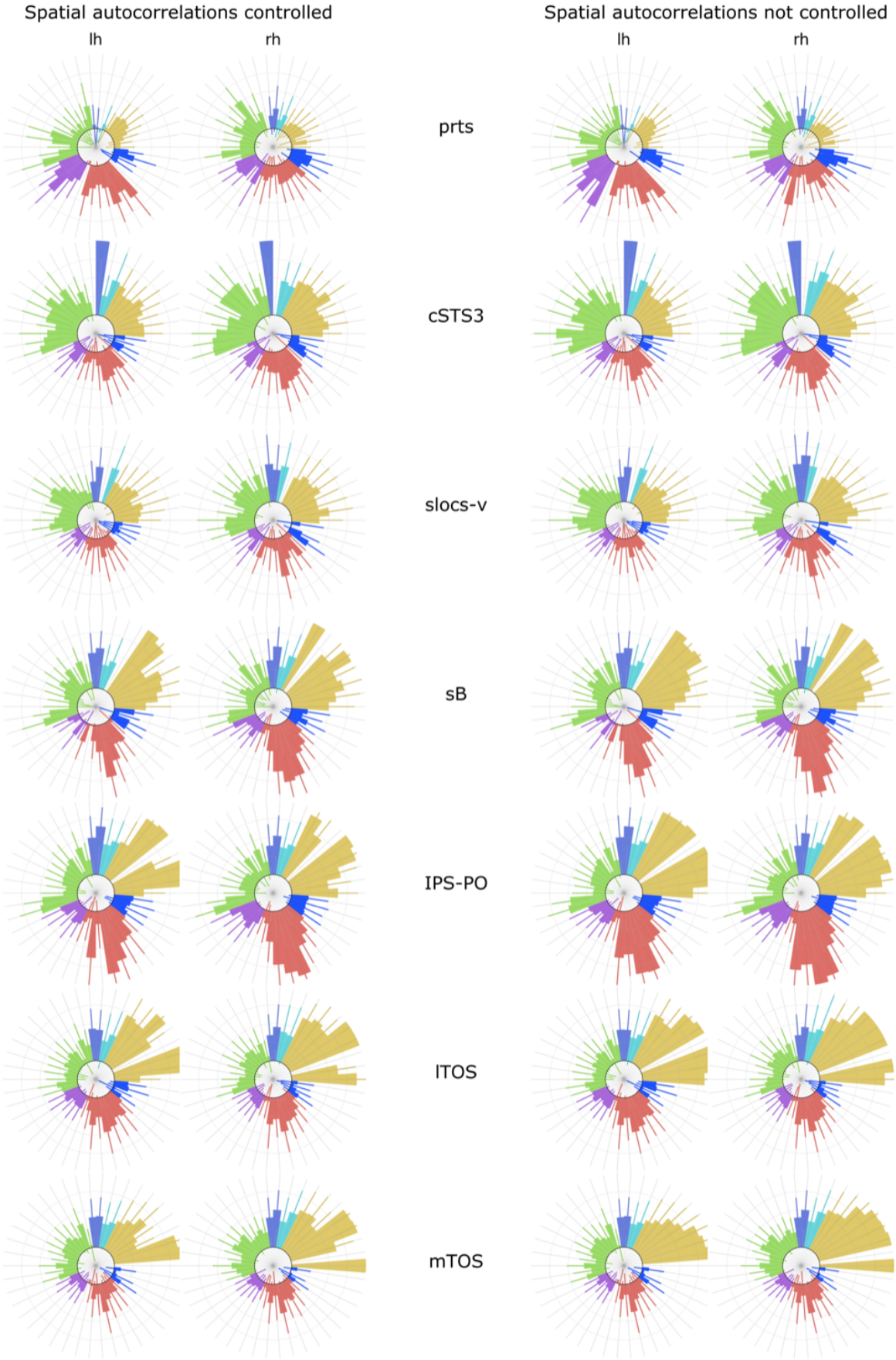
Spatial autocorrelations controlled
lh
rh
Spatial autocorrelations not controlled
lh
rh
prts
cSTS3
slocs-v
sB
IPS-PO
lTOS
mTOS

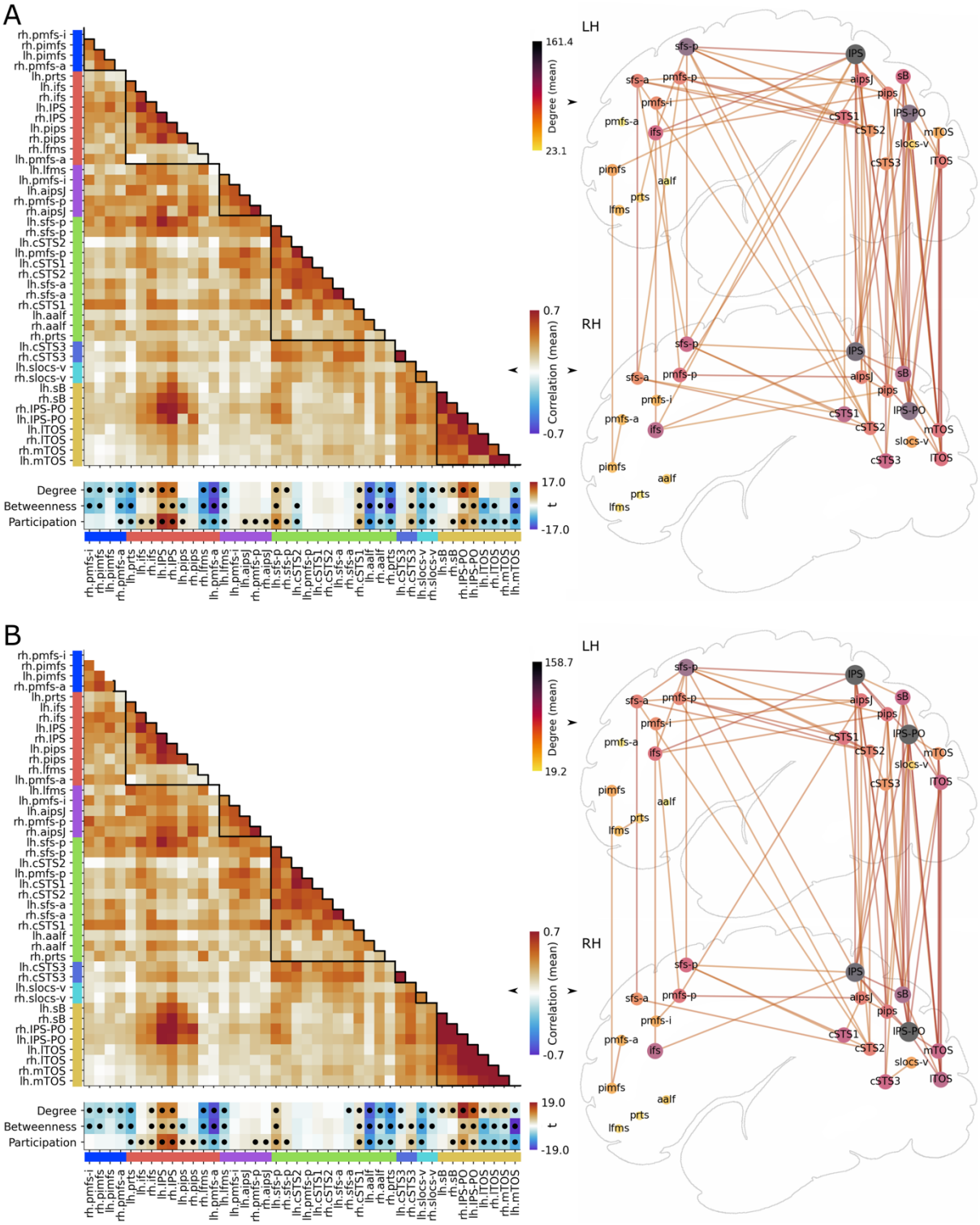

Extended Data Figure 3-2. Pairwise sulcal connectivity and graph analysis of LPFC and LPC sulci, with and without controlling for spatial autocorrelations. (A) Top left: Mean pairwise sulcal connectivity matrix. Black lines delineate pairs of sulci assigned to the same group-level cluster. Pairwise connectivity often appears strong for sulci assigned to the same

group-level cluster. Bottom left: nodes associated with significantly higher or lower degree, betweenness, or participation coefficient relative to the mean of values of all nodes for a given participant (same as **Figure 3C**). Cells are shaded according to strength of t-values for each comparison, with warm and cool colors denoting above and below mean. Black dots depict cells with significant (FDR-corrected $p < 0.05$) results when controlling for spatial autocorrelations. The cluster colors match **Figure 2B**. Right: Anatomical layout showing the strongest sulcal connections (0.10 density). Node size and color reflect mean degree.

(B) Results of a corresponding analysis when not controlling for spatial autocorrelations.

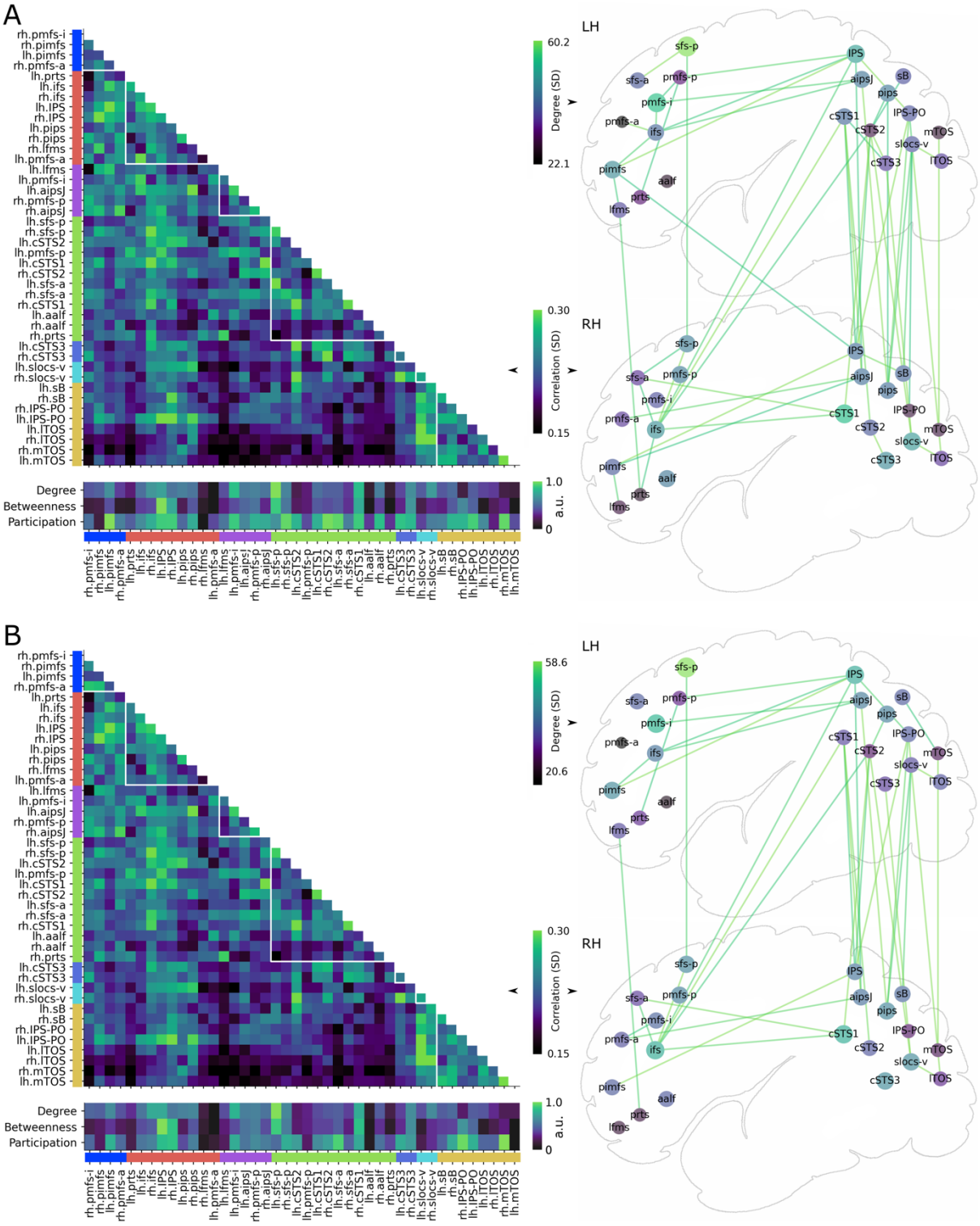

Extended Data Figure 3-3. Individual variability in the strength of pairwise functional connectivity of LPFC and LPC sulci, with and without controlling for spatial autocorrelations. (A) Top left: Individual variability in the strength of pairwise sulcal connectivity. Cells are shaded according to standard deviation, with brighter colors denoting

higher variability. White lines delineate pairs of sulci assigned to the same group-level cluster. Bottom left: Individual variability in degree, betweenness, and participation coefficient per sulcus, scaled to [0,1] across nodes. a.u.: arbitrary units. Right: Anatomical layout showing the connections within 15% of maximum. (B) Results of a corresponding analysis when not controlling for spatial autocorrelations. The anatomical layout shows connections within 30% of maximum.

Extended Data Table 4-1. Associations between depth and graph centrality for pTS of interest in LPFC, controlling or not controlling for age and spatial autocorrelations

		Spatial autocorrelations controlled			Spatial autocorrelations not controlled		
Sulcal component	Measure	t	p	p, FDR corrected	t	p	p, FDR corrected
lh.pimfs	degree	2.627	0.012	0.044*	2.529	0.015	0.040*
	betweenness	2.159	0.037	0.083	2.412	0.021	0.046*
	participation	1.995	0.053	0.106	1.809	0.078	0.140
rh.pimfs	degree	1.655	0.106	0.159	1.472	0.149	0.216
	betweenness	1.329	0.191	0.230	0.978	0.334	0.354
	participation	1.414	0.165	0.229	0.704	0.486	0.486
lh.pmfs-a	degree	1.328	0.192	0.230	1.386	0.174	0.217
	betweenness	1.672	0.102	0.159	1.710	0.095	0.156
	participation	1.098	0.279	0.314	1.362	0.181	0.217
rh.pmfs-a	degree	2.670	0.011	0.044*†	2.909	0.006	0.025*†
	betweenness	3.370	0.002	0.015*†	2.845	0.007	0.025*†
	participation	2.382	0.022	0.064	3.036	0.004	0.025*†

lh.pmfs-i	degree	3.437	0.001	0.015*†	3.586	0.001	0.011*†
	betweenness	2.869	0.007	0.039*†	3.480	0.001	0.011*†
	participation	2.332	0.025	0.064	2.685	0.011	0.032*†
rh.pmfs-i	degree	0.851	0.400	0.423	1.446	0.156	0.216
	betweenness	1.777	0.083	0.150	2.229	0.031	0.063
	participation	0.494	0.624	0.624	1.199	0.238	0.267

*Significant at FDR-corrected $p < 0.05$

†Significant when not controlling for age at $p < 0.05$, FDR-corrected

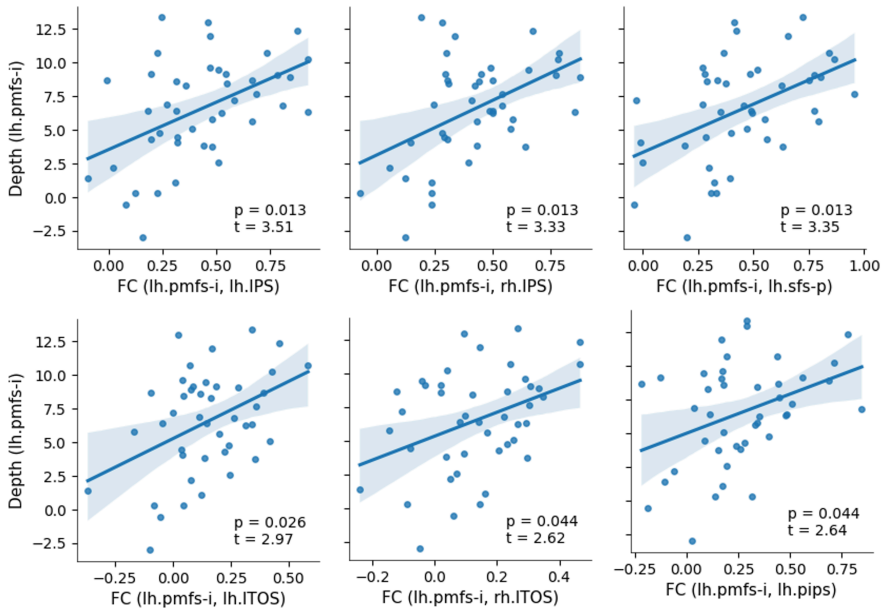

Extended Data Figure 4-1. Correlations between sulcal depth and pairwise functional connectivity. Partial regression plots illustrate relationships between depth and pairwise connectivity, after regressing out age, for each of the significant associations (i.e., those surviving FDR-correction, indicated with black dots in **Figure 4A**) – all of which involved lh.pmfs-i. Shaded areas represent 95 % confidence intervals. The plots are ordered from lowest to highest p-value.

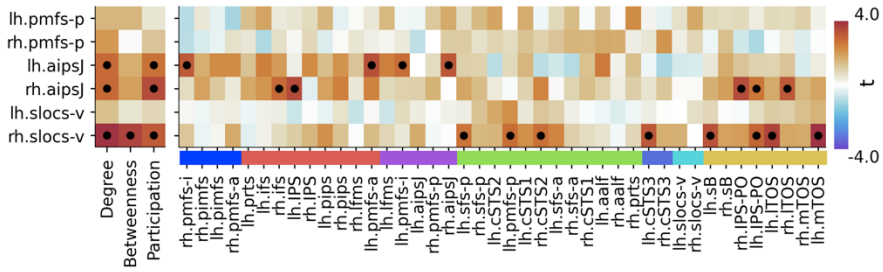

Extended Data Figure 4-2. Exploratory analyses testing associations between sulcal depth and connectivity for additional pTS of secondary interest (pmfs-p, aipsJ, and slocs-v), controlling for age in addition to spatial autocorrelations. Left-most columns: results of regression analyses testing associations between depth and centrality measures. Cells are shaded according to the strength of t-values for each regression, with warm and cool colors denoting positive and negative correlation, and darker shades indicating higher values. Dots depict cells with significant result (FDR-corrected $p < 0.05$). Columns at right: correlations between the depth of each of these sulci and the strength of their pairwise functional connectivity with the other sulci.